The Effect of Pressure and Particle Size on the Hydrodynamic Behavior of Particles in Semi-circular Fluidized Bed

by

Norliza Binti Mat Sidik

Dissertation submitted in partial fulfillment of
the requirements for the
Bachelor of Engineering (Hons)
(Chemical Engineering)

SEPTEMBER 2011

Universiti Teknologi PETRONAS
Bandar Seri Iskandar
31750 Tronoh
Perak Darul Ridzuan.

CERTIFICATION OF APPROVAL

The Effect of Pressure and Particle Size on the Hydrodynamic Behavior of Particles in Semi-circular Fluidized Bed

by

Norliza Binti Mat Sidik

A project dissertation submitted to the
Chemical Engineering Department
Universiti Teknologi PETRONAS
in partial fulfillment of the requirement for the
BACHELOR OF ENGINEERING (Hons)
(CHEMICAL ENGINEERING)

Approved by,

Dr. Ku Zilati Ku Shaari
Senior Lecturer
Chemical Engineering Department
Universiti Teknologi PETRONAS

(Dr. Ku Zilati Binti Ku Shaari)

UNIVERSITI TEKNOLOGI PETRONAS
TRONOH, PERAK
SEPTEMBER 2011

CERTIFICATION OF ORIGINALITY

This is to certify that I am responsible for the work submitted in this project, that the original work is my own except as specified in the references and acknowledgements, and that the original work contained herein have not been undertaken or done by unspecified sources or persons.

(NORLIZA BINTI MAT SIDIK)

ACKNOWLEDGEMENT

Bismillahirrahmanirrahim, Alhamdulillah. Thanks to Allah SWT, whom with His willing giving me the opportunity to complete this Final Year Project.

I would like to take this opportunity to acknowledge all parties who have contributed in making this final year research project a success. My deepest gratitude is dedicated to my supervisor, Dr. Ku Zilati Binti Ku Shaari, whose ideas were never failed to impress me and endless supports and encouragement given throughout the duration of two semesters. I am thankful to the the Coordinator of Final Year Project; Dr. Lukman Bin Ismail.

Special thank also goes to Chemical Engineering Lab Technologists; Mr. Muhammad Firdaus Bin Mohd Hashim and Mr. Mohd Jailani Bin Kassim for their help in laboratory works. I would like to extend my greatest appreciation to Dr. Lau Kok Keong from Chemical Engineering Department for lending the fluidized bed equipment and Assoc. Prof. Ir. Dr. Shaharin Anwar Sulaiman from Mechanical Engineering Department for lending the high speed camera and Mr. Khairul Anwar Bin Hj Ahmad and Mr. Mohd Fahmi Bin Ahmad Razali for their assistance during high speed photography training session. Also Professor Dr. Morgan Raymond Heikal and Mr. Firmansyah from Center for Automotive Research for the ideas exchange through discussions and devoted helps granted during image analysis.

I would also like to thank my colleagues; Mr. Luqman Hakim Bin Hassan and Ms. Yon Norasyikin Samsudin for all their support and help throughout the project. Lastly, I offer my regards and blessings to family and all of those who supported me in any respect during the completion of the project.

Thank you

ABSTRACT

Numerous investigations have been devoted towards understanding the hydrodynamics of particles in fluidized beds. However, most of them paid little to the behavior of coarse particles inside the fluidized bed. The present work aims to study the influence of pressure and particle size on the hydrodynamic behavior in fluidized bed processing. A semicircular fluidized bed, constructed from acrylic glass, with a vertical jet nozzle located at the centre of the distributor was used in the work. A high speed camera with a speed up to 3000 frames per second will be used to capture the images of fluidization process and it will make it possible to track the individual particle motion. The influence of pressure and particle size on the hydrodynamics can be determined using visualization by means of high speed photography and video imaging. Therefore the finding of this investigation will be helpful in understanding the reaction and determining the quality of fluidization and can be applied to achieve the best process design and optimum system operation.

TABLE OF CONTENTS

ACKNOWLEDGEMENT i

ABSTRACT ii

TABLE OF CONTENT iii

LIST OF FIGURES v

LIST OF TABLES vi

CHAPTER 1: INTRODUCTION 1

1.1 Background Study 1

1.1.1 Fluidized bed Development . . 2

1.2 Problem Statement 4

1.3 Objectives & Scope of Investigation . . 5

CHAPTER 2: LITERATURE REVIEW 6

2.1 Earlier Study on Fluidized Bed . . . 6

2.2 High Speed Photography and Digital Image Analysis 10

CHAPTER 3: METHODOLOGY 14

3.1 Experimental System 14

3.2 Experimental Procedure . . . 15

3.3 Image and Data Analysis . . . 18

3.3.1 Void Fraction, ε . . . 18

3.3.2 Bed Expansion, δ . . . 19

3.3.2 Bubble Diameter . . . 20

CHAPTER 4: RESULTS & DISCUSSION . . . 21

4.1 Void Fraction, ε 21

4.2 Bed Expansion, δ 22

4.3 Bubble Diameter 24

CHAPTER 5: CONCLUSION & RECOMMENDATION . 27

REFERENCES 29

APPENDICES 32

LIST OF FIGURES

Figure 1: Bed pressure drop vs. air flow rate 1
Figure 2: Bed expansion vs. velocity. 3
Figure 3: (a) Particle fluidization structure 6
Figure 4: Six distinct flow patterns 11
Figure 5: (a) original image (b) binary image. 12
Figure 6: Fluidized bed equipment 14
Figure 7: Experimental setup 15
Figure 8: Procedure 16
Figure 9: GSA image analyzer interface 18
Figure 10: Urea 2.36mm bed height, H at different pressure . . . 19
Figure 11: Bubble diameter for bed of sand 1.64 mm at different pressure . 20
Figure 12: Void fraction vs. air pressure 22
Figure 13: Bed expansion vs. air pressure 23
Figure 14: Bubble diameter at different pressure for sand (1.64 mm) . 24
Figure 15: Bubble diameter at different pressure for urea (2.36 mm) . 25
Figure 16: Bubble diameter at different pressure for urea (3.35 mm) . 25
Figure 17: Average bubble diameter for different particles . . . 26
Figure 18: Sand 1.64 mm bed height, H at different pressure . . 32
Figure 19: Urea 2.36mm bed height, H at different pressure . . . 33
Figure 20: Urea 3.35mm bed height, H at different pressure . . . 34
Figure 21: Bubble diameter for bed of sand 1.64 mm at different pressure . 35
Figure 22: Bubble diameter for bed of urea 2.36 mm at different pressure . 37
Figure 23: Bubble diameter for bed of urea 3.35 mm at different pressure . 39

LIST OF TABLES

Table 1: Experimental matrix 17
Table 2: Void fraction for sand (1.64 mm) 21
Table 3: Void fraction for urea (2.36 mm) 21
Table 4: Void fraction for urea (3.35 mm) 21
Table 5: Bed expansion for sand (1.64 mm) 22
Table 6: Bed expansion for urea (2.36 mm) 22
Table 7: Bed expansion for urea (3.35 mm) 23
Table 8: Bubble diameter for bed of sand 1.64 mm at different pressure . 36
Table 9: Bubble diameter for bed of urea 2.36 mm at different pressure . 38
Table 10: Bubble diameter for bed of urea 3.35 mm at different pressure . 40
Table 11: Project activities of FYP I 41
Table 12: Project activities of FYP II 41

CHAPTER 1

INTRODUCTION

1.1 Background Study

In fluidization, a gas is passed through a bed of solid particles which is supported on a perforated or porous plate. When the frictional force acting on the particles or pressure drop of the flowing air through the bed equals or exceeds the weight of the bed, the particles become suspended and the bed exhibits liquid-like behavior. At gas flow rates less than the fluidization velocity, the bed is a fixed bed and there is no movement of particles. At flow rates above minimum fluidization the bed expands and bubbles appear.

The air velocity corresponding to a pressure drop that just equals the weight of the bed is referred to as the minimum fluidization velocity (Hesketh et al., 2002). At this air velocity or flow rate all of the bed particles are completely suspended by the air stream. For a given system, minimum fluidization velocity can be determined from a pressure drop versus air velocity diagram.

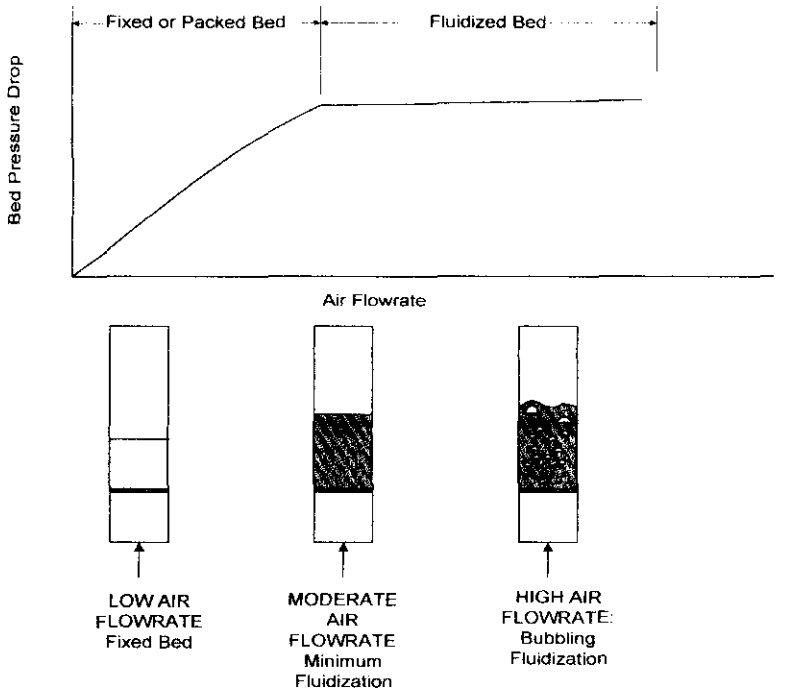

As air flow is increased above the minimum fluidization velocity, the bed may exhibit behaviors ranging from smooth fluidization to bubbling fluidization to dilute fluidization in which powder can be transported by the air stream.

The two-phase fluidization occurs in many industrial and environmental processes. These include pharmaceutical, petrochemical, and mineral industries, energy conversion, and gaseous and particulate pollutant transport in the atmosphere, heat exchangers, and many other applications. The gas-solid fluidized bed reactor has been used extensively because of its capability to provide effective mixing and highly efficient transport processes.

1.1.1 Fluidized Bed Development

The first reactor based on the principles of fluidized bed technology; bubbling fluidized bed was constructed in 1950 for roasting of sulfur bearing materials. The new system was quickly adopted by industry such as multiple hearth furnaces and rotary kilns were increasingly replaced by fluidized bed roasters, thereby ensuring enhanced product quality and significantly reduced plant emissions.

The classical bubbling fluidized bed (FB) is operated at relatively low gas velocities with the particles kept in balance against their own gravity. Most of the particles do not leave the surface of the fluidized bed, typically characterized by a defined surface between gas and solids. The surface may show a behavior similar to a boiling liquid, depending on size and density of the particles. From the mixing point of view, the FB is a continuously stirred tank reactor with a defined solids residence time distribution. The mean solid velocity is close to zero with the slip velocity almost identical to the gas velocity.

Fluidized bed combined with efficient heat recovery and off-gas treatment, including the process of converting the off-gas to sulfuric acid, became state-of-the-art technology for processing sulfur bearing ores. Significant process improvements have been achieved by using fluidization technology, for example in the production of alumina.

The circulating fluidized bed (CFB) was developed in 1959 for the high temperature treatment of fine and light particles. A whole variety of other CFB applications followed, with more than 170 industrial plants worldwide. The CFB has been successfully applied for coal combustion, roasting of gold containing ores, direct reduction of iron ore fines and other uses.

At higher gas velocities the slip velocity increases and the fluidized bed changes its behavior. The defined boiling surface disappears with the expansion of the fluidized solids. The fluidization gas has enough energy to entrain solids particles. The entrained particles are separated from the gas by a cyclone and recirculated via an external loop back into the fluidized bed reactor. In addition an internal recirculation of the solids in the fluidized bed reactor takes place. Both internal and external circulation results in a homogenous temperature distribution in the CFB system.

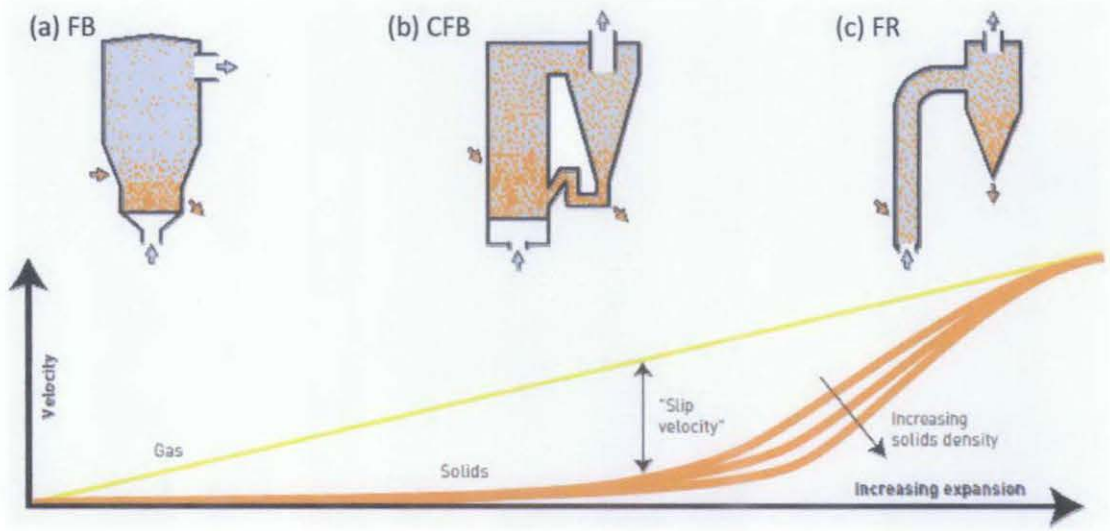

Figure 2: Bed expansion vs. velocity

In 1985, flash reactor (FR) for high temperature alumina production was developed. With further increase of the gas velocity, the solids are approaching the velocity of the gas. In the flash reactor the slip velocity between gas and solids is considerably decreased compared to the circulating fluidized bed. At the same time the advantages of homogeneous temperature distribution and ideal heat and mass transfer are decreased.

In the early 1990s, a new variation of fluidization technology was introduced; the annular fluidized bed (AFB).This new type of fluidized bed improves the introduction

and mixing of hot dust laden process gases. These gases enter the reactor through a large central nozzle, with additional fluidization gas introduced through an annular nozzle ring. As a result, a very intense mixing zone is achieved within the reactor above the central nozzle, comparable to the conditions achieved by an external loop of a CFB. Further advantages are excellent process control and improved mass transfer conditions. The AFB can be combined with any other fluidized bed type.

1.2 Problem Statement

The gas-solid flows at high concentration in these reactors are quite complex because of the coupling of the turbulent gas flow and fluctuation of particle motion dominated by inter-particle collisions, which lead to considerable difficulties in designing, scaling up, and optimizing the operation of these reactors.

Despite a significant amount of research on fluidized bed reactors, there are considerable uncertainties on their behavior. The fundamental problem encountered in modeling the hydrodynamics of a gas-solid fluidized bed is the strong interaction of the phases with unknown and transient interfaces. As a result, the interaction of the phases is understood only for a limited range of conditions. One additional important complexity is that in many of these industrial processes the gas flow is in a turbulent state of motion.

Fluidized beds have also been subjected to many experimental and theoretical investigations. However these studies paid little attention to the coarse particles behavior inside the bed. This provides the motivation of a systematic investigation into the solids behavior in the jet region of gas fluidized beds.

Although many investigations have been done, little attention is paid to the behavior of coarse particles inside the fluidized bed. Until 1970s, very little is published on the influence of pressure on the operation of the fluidized bed processes.

1.3 Objectives & Scope of Investigation

The objectives of the research are:

i. To study the influence of pressure on the hydrodynamic behavior in fluidized bed processing.

ii. To study the effect of particles size on the hydrodynamic behavior in fluidized bed processing.

The hydrodynamic behavior can be described in term of voidage, bed expansion and bubble diameter. Since the hydrodynamics of gas-solids mixtures in fluidization are very complex, visualization by means of high speed photography and video imaging enables a better understanding of the mechanics of these processes. The development and use of high speed photography, video imaging and image analysis has enabled capturing fast moving images without a blurring effect, especially in the measurement of bubble movement.

In this work, a high speed camera with high frame frequency will be used to capture the images of fluidization process and it will make it possible to analysis the characteristics of particles inside the bed.

CHAPTER 2

LITERATURE REVIEW

2.1 Earlier Study on Fluidized Bed

Flow pattern of the fluidized bed is important to comprehend the fluidization conditions because the complex correlation between particle-particle and particle-environment in the reactor. In their study, Wang and Ren (2009) applied acoustic emission (AE) measurement in monitoring the particle fluidization pattern in a gas-solid bed fluidized with different sorts of particles classified by Geldart. With AE axial time average energy analysis, the flow structure of polyethylene particles was investigated both in the laboratory and plant apparatus. The results showed that the fluidization pattern in the bed is multi-circulation, including the main-circulation zone, sub-circulation zone, and the stagnant zone.

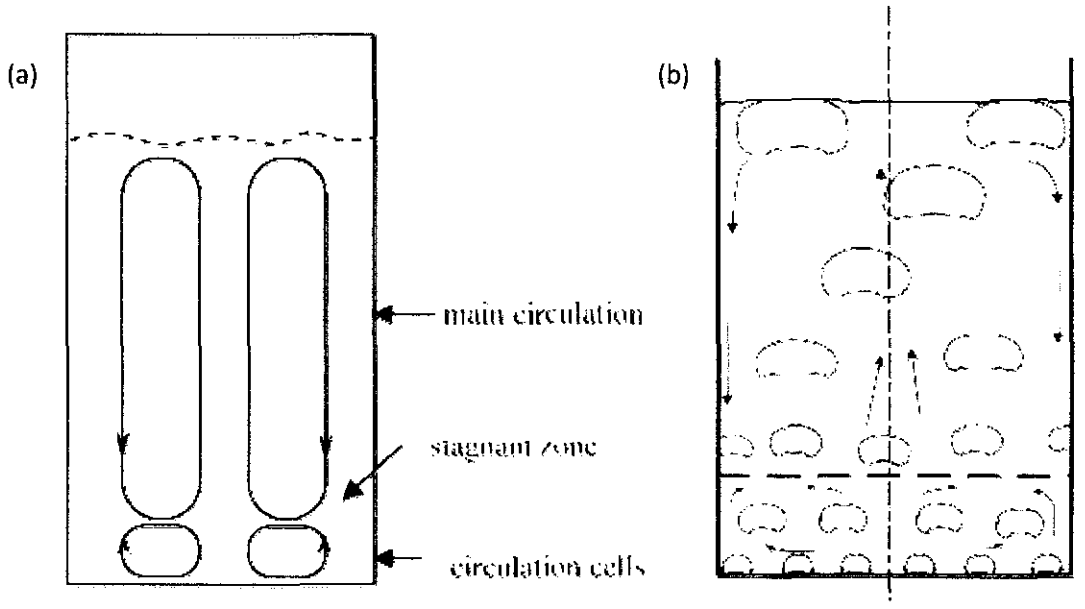

Moreover, the influence of operating variables, such as particle size, superficial gas velocity, static bed height, and particle sorts had also been considered. It was found that the particle size, gas velocity, and particle sorts have significant impacts to the fluidization pattern. In contrast, the height of the stagnant zone did not show direct

relation to the static bed height. AE measurement was proved to be reliable for understanding the dynamical features that affect the behavior of the fluidized bed. This can be useful guidance for an industrial process and help improve the process operation and the design of the new reactor.

Unsteady-state heat transfer and hydrodynamics in a gas-solid fluidized-bed reactor has been investigated by Hamzehei and Rahimzadeh (2009). Simulation results show that small bubbles are produced at the bottom of the bed. These bubbles collide with each other as they move upward, forming larger bubbles. The influence of the size of the solid particles on the gas temperature is also studied. For smaller particle sizes, because of a higher heat-transfer coefficient between the gas phase and the solid phase, the solid phase temperature rapidly increases and the mean gas temperature rapidly decreases. To validate the model, predicted pressure drops and gas temperature variation are compared to corresponding values of experimental data. The modeling predictions compared reasonably well with experimental data.

A recent work by Subramaniam (2003) focused on evaluating the effect of tablet deflectors in the spray zone on the variation of coating material received by individual tablets as they pass through the spray. Digital video imaging is used to illustrate how different type of deflectors changed the solid velocity and voidage profile near the spray nozzle. The major effect of the tablet deflectors is to increase the voidage in the vicinity of the spray zone and hence reduce the local wetting phenomenon that is known to occur close to the spray source.

Hydrodynamic characteristics such as bed expansion and pressure drop of low-density polyethylene (LDPE) and polypropylene (PP) are studied by Vijaya Lakshmi (2000) in a liquid-solid inverse fluidized bed reactor as a function of particle diameter, liquid viscosity and density. The bed expansion and pressure drop data are used to determine the minimum fluidization velocity, U_{mf} and friction factor, f. It was found that the U_{mf} increased with an increase in the particle diameter and a decrease in solid density and was independent of initial bed height or solid loading. In addition, the U_{mf} decreases with an increase in the liquid concentration. The friction factor Reynolds number plot is found similar to that of classical fluidization.

An initial increase in bubble size or volume in the lower pressure range up to 1000kPa (Rowe et al., 1984) and 1600kPa (Hoffmann and Yates, 1986) and decrease thereafter up to 8100kPa is observed. This is more or less consistent with the results of Olowson and Almstedt (1990) who studied the hydrodynamics in a freely bubbling pressurized fluidized bed and observed the similar effect of pressure on the mean pierced length of bubbles for coarse sand, which at atmospheric pressure is close to Geldart B/D boundary. However, their pressure range was between atmospheric and 1600 kPa and the mean pierced length of bubbles reached a maximum at around 400 kPa. In a later paper (1992), they stated that an increase in pressure may either cause an increase or a decrease in bubble size, depending on the location in the bed, gas velocity and the pressure level; and the bubble size is determined by a complex balance between coalescence and splitting.

Correlations for hydrodynamic properties such as pressure drop, bed expansion, and minimum fluidization velocity in turbulent bed contactors are presented by Vunjak-Novakovic and Vukovic (1987). The correlations are very dependent on the bed operating regime. Only the operating liquid holdup contributes to the bed pressure drop. For each operating regime, there are three regions on the curve of bed expansion vs. gas velocity: the packed-bed, partially fluidized-bed, and the fully developed fluidized-bed regions. When U_{mf} is reached in the bed, it fluidizes and the interstitial gas velocity remains constant throughout the region of partial fluidization. The liquid holdup and the bed expansion adjust as the total flow increases. The hydrodynamic conditions change and the interstitial velocity begins to increase when the bed is fully fluidized.

Weimer and Quarderer (Weimer, 1986; Weimer & Quarderer, 1985) measured dense phase voidage and dense phase superficial gas velocity at pressures up to 8300 kPa in a pilot-scale fluidized bed of bubbling Geldart A and Geldart A/B boundary carbon powders. They found that the magnitude of the pressure effect on the dense phase voidage strongly dependent on particle size.

Chiba et al. (1986) fluidized sand of two sizes; 0.3 and 0.6 mm at atmospheric, 400 kPa and 800 kPa pressure and noticed that the bed expansion ratio clearly increase with pressure. The pressure effect was larger for the coarser particles, however at 800 kPa

the bed expansion ratio became almost the same for both materials. Chitester et al. (1984) visually studied bed expansion of coal, char and ballotini at atmospheric, 2169 kPa, 4238 kPa and 6306 kPa. In case of coal (Geldart B material), initial bed expansion occurred with a lower gas velocity at higher pressure and the bed expanded more at high pressures at a given gas velocity. However, for char (Geldart A powder) and ballotini (Geldart A/B boundary material), at a given gas velocity the bed expansion height did not always increase with pressure.

Piepers et al. (1984) carried the collapse experiments with 59 μm cracking catalyst and found that the dense phase voidage increased from 0.52 at atmospheric pressure to 0.58 at 1500 kPa, which is more in line with the observations of Weimer and Quarderer (1985). The quality of fluidization of abed of improves with pressure but is also dependent on the type of fluidization gas used. This can be explained by an increasing elasticity modulus of the powder structure with increasing pressure. The higher elasticity modulus is the result of an increase of the cohesion between the particles. This increase in cohesion is probably due to an increased gas adsorption to the solid at higher pressures.

Effects of gas and liquid velocities and particle density (polyethylene and polypropylene) on the immersed heater to-bed heat-transfer coefficient, individual phase holdup, and minimum liquid fluidization velocity have been determined by Cho and Park (2002). The minimum liquid fluidization velocity decreases with increasing gas velocity in the inverse fluidized beds. The gas and liquid holdups increase with an increase in the gas or liquid velocity in the beds. The heat-transfer coefficient in two and three-phase inverse fluidized beds of relatively high density particles (polyethylene) is higher than that in the beds of relatively low density particles (polypropylene). The heat transfer coefficient increases with increasing gas velocity; however, it exhibits a maximum value with increasing liquid velocity in liquid-solid as well as three-phase inverse fluidized beds. The liquid velocity at which the heat-transfer coefficient value attains its maximum value decreases with increasing particle density or gas velocity.

Circulating high-velocity fluidized beds (HVFB) have been proposed to eliminate some of the problems encountered in conventional fluidized beds. The loop fluidized bed

(LFB) is one such system being considered for pressurized combustion of coal in the presence of sulfur sorbent such as dolomite. The study conducted by Breault and Mathur (1989) to obtain fundamental knowledge of the hydrodynamics of the LFB which has been operated using sand, limestone, and gypsum particles. Experimental data are obtained to study the effect of particle size, particle density, air flux, and solid flux on the pressure profile in a circulating high-velocity fluidized bed. Based on the data, a pressure profile model represented by the computer program has been developed which accurately predicts pressure drop at any point in the LFB system.

Whittman and Ademoyega (1987) have measured some hydrodynamic changes in a two-dimensional gas fluidized bed when an external cross-flow dc field is applied. For a constant flow rate of bone-dry oxygen, when the electric field strength increases, the bed height increases linearly, the bubbles become elongated and can be idealized by ellipsoids with increasing eccentricity, their frequency decreases sharply, and their rising velocity decreases nearly linearly. With increasing field strength, the minimum fluidizing flow rate increases, implying that the dc field allows operation of the bed near minimum fluidizing conditions at much higher gas flow rates. For a given gas flow rate, the observed changes imply a decrease in the flow through the bubble phase as well as an increase in bubble residence time. When the electro-fluidized bed apparatus was used as a catalytic reactor, there was a linear decrease in ozone concentration in the exit stream.

2.2 High Speed Photography and Digital Image Analysis

Experiments are carried out by Ren et al. (2010) in a visible multiple-spouted bed, which is a combination of three spouted bed cells. Typical flow patterns by certain criteria as well as schematic diagrams and typical flow pattern images are determined. Flow regime maps at different static bed heights are studied. Besides, some important flow characteristics associated with this topic; minimum spouted velocity and bed pressure drop, are discussed. Figure 4 shows the images obtained from a high-resolution digital charge coupled device (CCD) camera.

The kind of flow pattern is different at different static bed heights, and most obviously, the flow pattern of internal jet with slugging only exists at a high static bed height. The central minimum spouting velocity increases with an increasing bed height, and auxiliary spouting gas has no effect on this trend. However, auxiliary spouting gas appears to affect remarkably the central minimum spouting velocity; the minimum central spouting velocity decreases with a low auxiliary spouting gas flow rate but increases with a high auxiliary spouting gas flow rate. The total bed pressure drop increases first and then decreases gradually with the auxiliary spouting gas at a certain central spouting gas flow rate, while the total pressure drop increases first and then remarkably decreases with the central spouting gas at a certain auxiliary spouting gas flow rate.

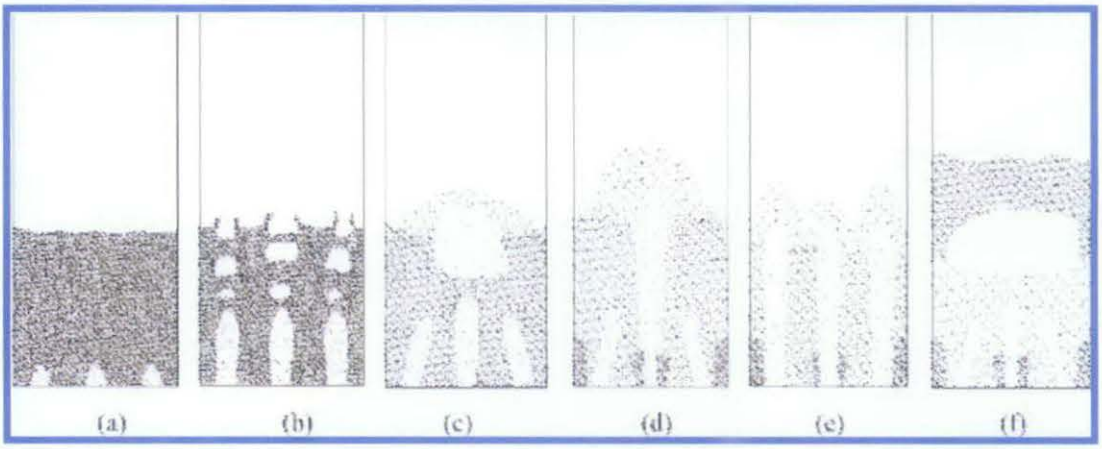

Figure 4: Six distinct flow patterns (a) fixed bed (b) internal jet (c) internal jet with bubble (d) single spouting (e) multi-spouting (f) internal jet with slugging (Ren et al., 2010)

A new method of digital image analysis has been developed by Shen and Johnsonn (2004) to study the hydrodynamics of two-dimensional bubbling fluidized beds with a digital video camera. The bed is uniformly illuminated by light sources to eliminate undesirable shadows and intensity gradients. Films on the bubbling fluidized bed are captured using CCD digital video camera which possesses several additional features including a variable shutter speed and auto/manual gain control. The high shutter speed feature is essential for capturing fast moving images without a blurring effect, especially in the measurement of bubble movement. The auto-gain feature of digital

video camera enables self-adjustment of the illumination level under the influence of the background or surrounding brightness.

The films are recorded in the Red, Green and Blue (RGB) format. The time duration of each process is about 8–10 min. And then the films of digital video image from the video camera are transferred to PC computer. The relative image area of the films is captured by an image frame-grabber. With the image processing toolbox of Matlab, computer software is developed to automate the procedures for image acquisition, data processing and analysis for frame by frame. Then the time-averaged data about bubble characteristics in the bed is acquired.

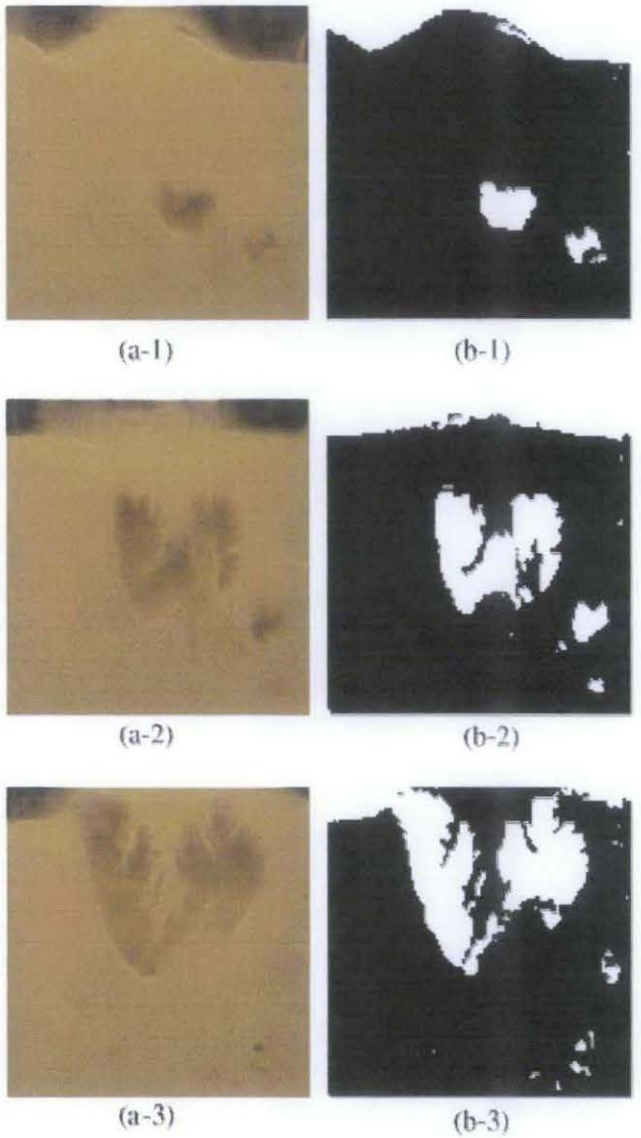

Figure 5: (a) original image (b) binary image (Shen and Johnsonn, 2004)

Figure 5 is an example of image processing of a bubbling fluidized bed. It shows the process that bubbles grow up, split and erupt at the bed surface. The time delay between the three frames is 4/50 s. Figure 5(a) is an original RGB image which is then converted to the gray one. The initial step in image processing involves the discrimination of bubbles from the emulsion phase. When the image contrast is sufficient, phase identification is made possible by assigning a threshold value. With the process of image enhancement, data reduction, and analyzing images to extract information about their structure, the RGB image is thresholded and then converted to the binary one. The binary segmentation mask of the bubbles is displayed in Figure 5(b). The white area in the bed is identified as bubble phase.

The threshold value has an impact on the detection of bubble boundaries. It is assessed through the comparison of a typical frame of the video film with the binary segmentation mask of bubbles. And then the value is chosen to be a universal threshold value, and be applied to the whole procedure of image processing. Image contrast of bubbling fluidized beds is normally high, the delineation of the bubble boundary with high accuracy is acquired. Thus the binary thresholded images are used to study the bubble characteristics in bubbling fluidized beds.

The detection and measurement of the bubble parameters are automated by employing a series of systematic edge searching routines. The initial step of the routine detects the number of the bubbles intersecting a line positioned at some height above the distributor. For every bubble detected, the complete boundary of the bubble may be delineated through further scanning across the image, as shown in Figure 5(b).

When a large bubble has started to erupt at the bed surface, the boundary of the bubble at the bed surface is incomplete, as shown in Figure 5(b-3). To establish such a bubble boundary, the complete boundary of bed surface at the moment should be evaluated, based on the polynomial or interpolation. And then the boundary of such a bubble could be delineated. One of the measured bubble parameters is the white projected area of the bubble. Bubble density, δ_b can be inferred as follows:

$$\delta_b = \frac{white\ projected\ area}{specified\ area}$$

CHAPTER 3

METHODOLOGY

3.1 Experimental System

The visible fluidized bed experimental system is schematically shown in Figure 6 and 7, which includes a gas supply system, fluidized bed equipment, and a charge coupled device (CCD) imaging system. The column has an outer diameter of 70 mm and inner diameter of 60 mm and a height of 500 mm. The column is made of 5 mm-thick transparent Plexiglas. A 10 mm diameter nozzle is inserted vertically in the middle of the distributor for the introducing a jet continuously. The central spouting gases were supplied by an air compressor.

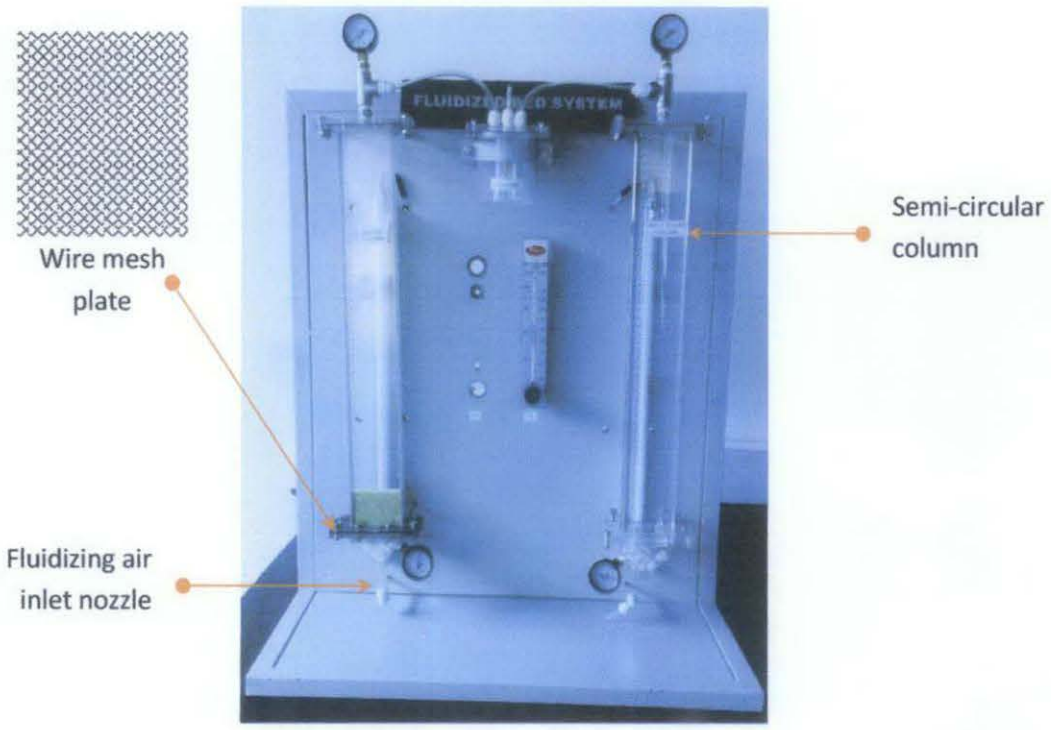

Figure 6: Fluidized bed equipment

A high-speed digital camera with a high-speed consecutive shooting rate of up to 3000 frames per seconds in JPEG format is used. It will meet the need of capturing a series of the gas-solid flow structure. To obtain photographs as vivid as possible, the column was

illuminated by two 2000 W floodlights, one on each side for uniform lighting. Sand and urea granules are used as bed material and air as the fluidizing gas supplied by a compressor.

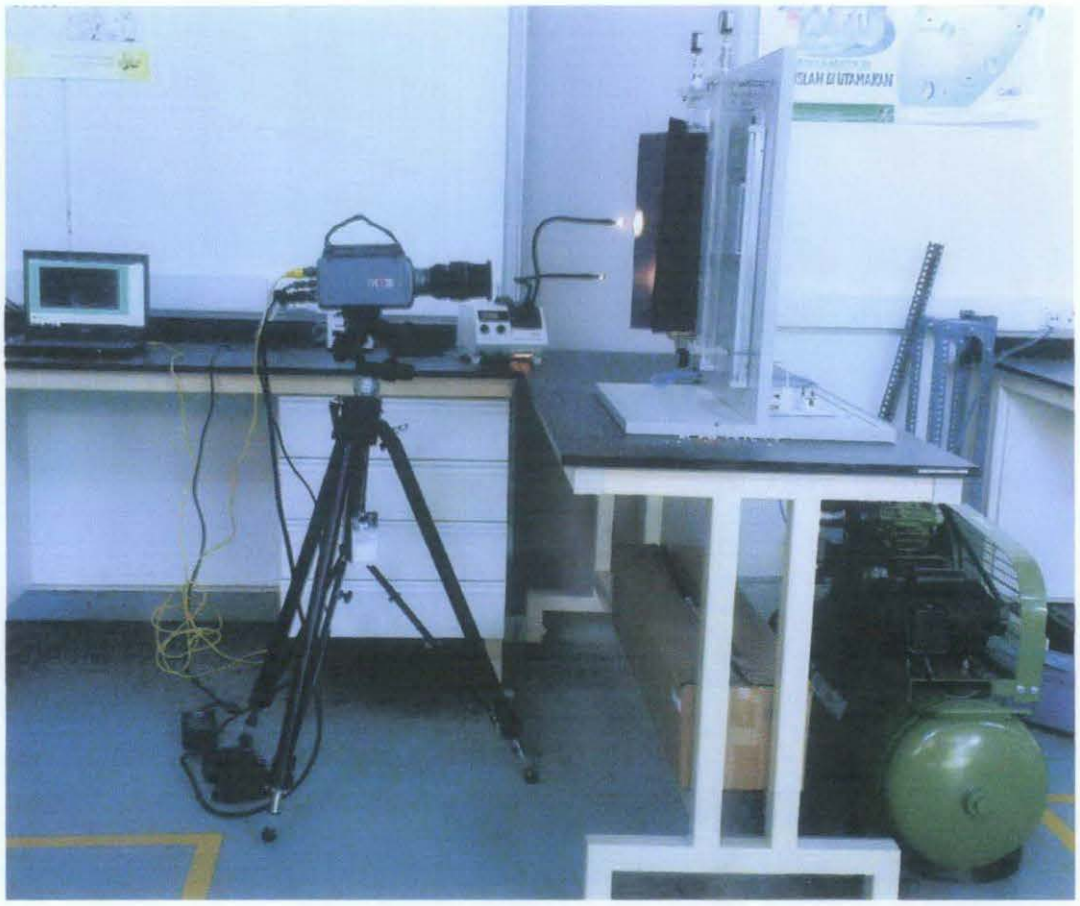

Figure 7: Experimental setup

3.2 Experimental Procedure

Once all equipments are set up as in Figure 6, they are ready to be used for the experiment. First, the sand particles are loaded into the semi circular column until it reaches 8 cm height. Then, the upper cap of the column is replaced and tightened to ensure no leaking. Then, the air compressor is started to supply the fluidizing air to the bed through the inlet nozzle located at the bottom of the column. Air is passed through the particles bed and maintained at the minimum fluidization state.

Then, the air pressure is adjusted and set to 1 bar and the bed is left to fluidize. During fluidization, the process is recorded using the high speed camera which is set at 3000 frames per seconds. The images captured are saved to be analyzed. The experiment is repeated using the same bed of sands at different fluidizing air pressure; 0.75 bar, 0.5 bar and 0.25 bar. Then, the sand particles are removed from the column.

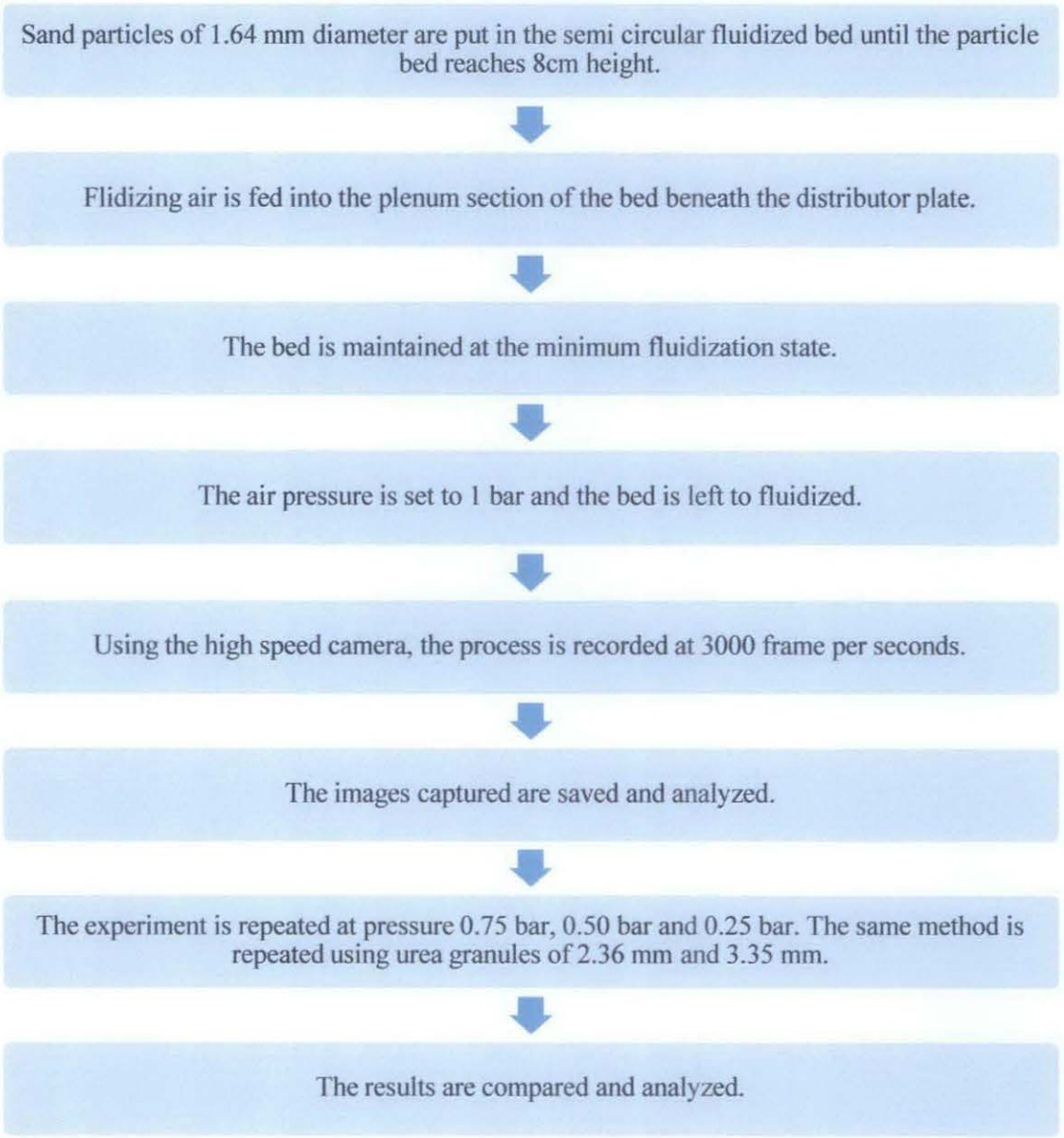

Figure 8: Procedure

The whole steps are repeated using urea granules of 2.36 mm and 3.35 mm in diameter. The detailed condition of each experimental run is shown in Table 1.

Table 1: Experimental matrix

Experiments	Type of Particle	Particle Diameter (mm)	Fluidizing Air Pressure (bar)
Run 1	Sand	1.64	1.00
			0.75
			0.50
			0.25
Run 2	Urea	2.36	1.00
			0.75
			0.50
			0.25
Run 3	Urea	3.35	1.00
			0.75
			0.50
			0.25

3.3 Image and Data Analysis

The images obtained from each experimental run are analyzed based on the methods that will be further described below.

3.3.1 Void Fraction, ε

Void fraction is defined as the ratio bubble area to the total bed area. An original image can be converted to binary image using GSA Image Analyser software and the detailed steps are as discussed in the literature review. From the binary image, the software will automatically calculate the bubble and total bed areas.

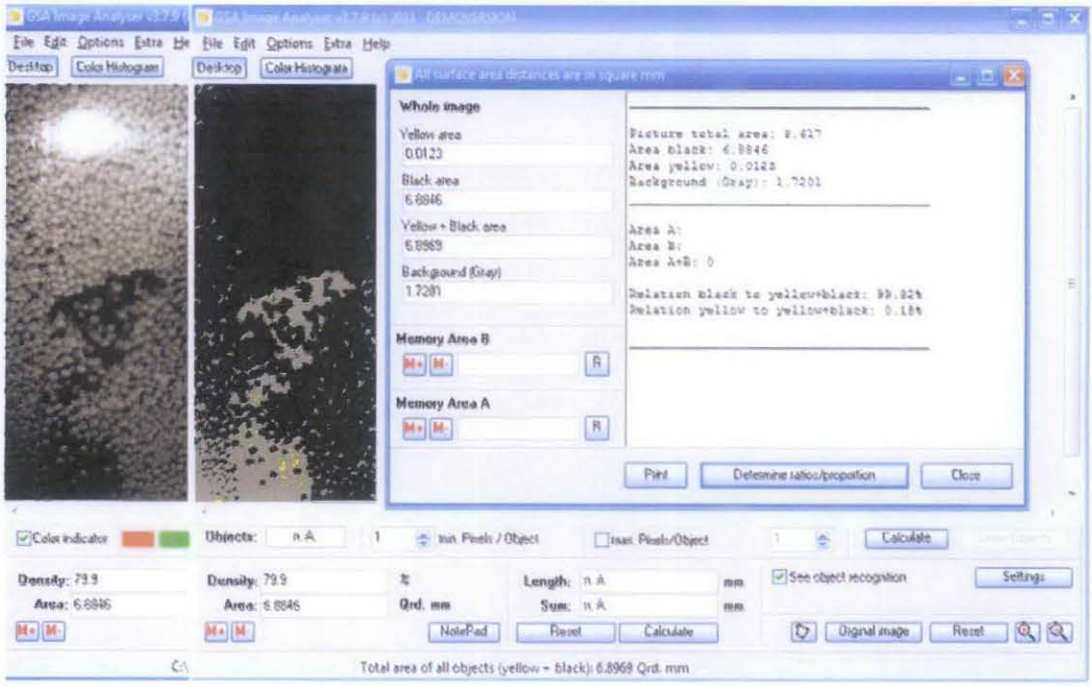

Figure 9: GSA image analyzer interface

In Figure 8, the original image is on the left and the binary image is on the right hand side. The pop-up window shows the areas calculated. The bubble is denoted as gray area and the particles are the black and yellow area. In this example, the bubble area is 1.7201 mm^2 while the particle area is 6.8969 mm^2.

Using the equation below, the void fraction can be calculated.

$$\varepsilon = \frac{gray\ projected\ area}{specified\ area} = \frac{bubble\ area}{total\ bed\ area} = \frac{1.7201}{1.7201 + 6.8969} = 0.2$$

3.3.2 Bed Expansion, δ

Bed expansion of a fluidized bed is expressed as the ratio of bed height, H to the initial bed height, H_{mf} measured at the minimum fluidization. Olowson and Almstedt (1990) and Wiman and Almstedt (1998) described the bed expansion as the following equation:

$$\delta = \frac{H - H_{mf}}{H}$$

At different pressure, the images below are captured. The bed height at minimum fluidization of the 2.36 mm-diameter urea granules, H_{mf} is 8.9 cm.

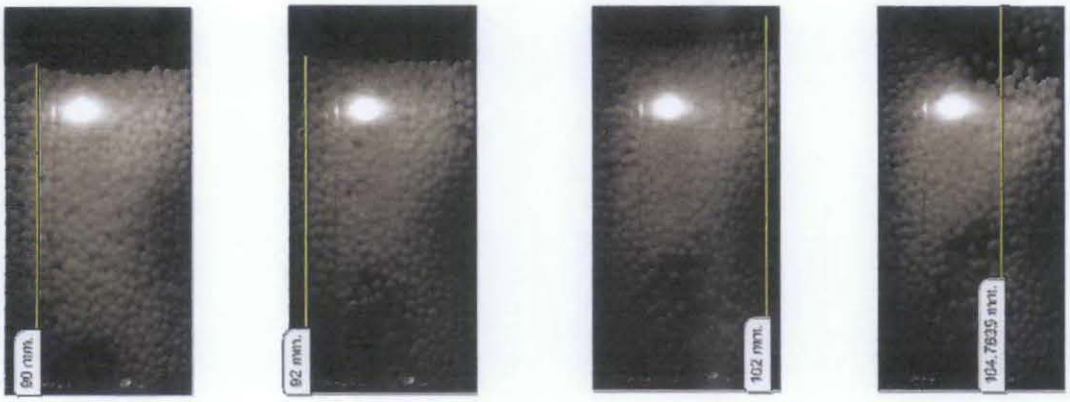

Figure 10: Urea 2.36mm bed height, H at different pressure; (a) 0.25 bar (b) 0.5 bar (c) 0.75 bar (d) 1 bar

The bed expansion can be determined as follows;

$$At\ P = 0.25\ bar, \qquad \delta = \frac{H - H_{mf}}{H} = \frac{(9.0 - 8.9)cm}{9.0\ cm} = 0.011111$$

3.3.3 Bubble Diameter

The diameter of the bubble is measured at every 0.5 cm along the bed height. The data for each is compiled in a table and the average bubble diameter can be calculated.

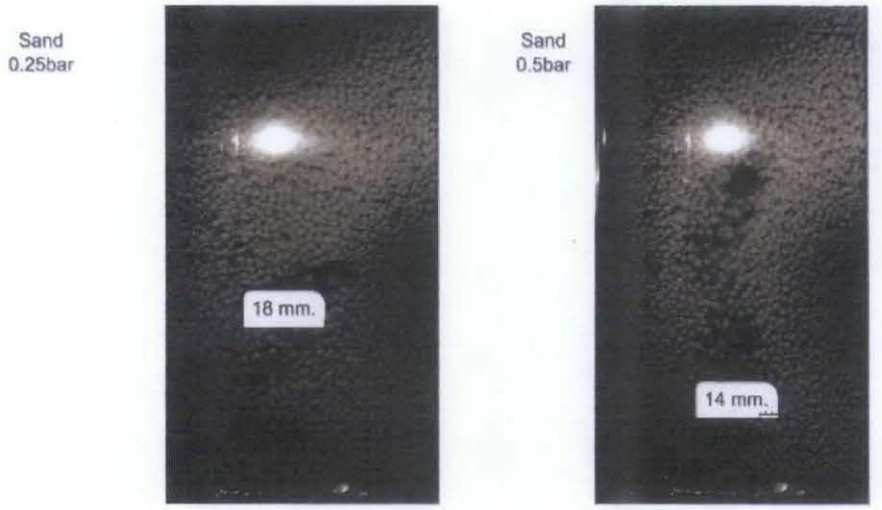

Figure 11: Bubble diameter for bed of sand 1.64 mm at different pressure

CHAPTER 4

RESULTS & DISCUSSION

4.1 Void Fraction, ε

Void fraction of the bed for each experimental run is calculated and shown in Table 2-4.

Pressure (bar)	Particle Area (mm^2)	Bubble Area (mm^2)	Total Area (mm^2)	ε
0.25	6.8969	1.7201	8.617	0.200
0.50	6.7111	1.9059	8.617	0.221
0.75	6.6837	1.9334	8.617	0.224
1.00	5.4989	3.1181	8.617	0.362

Pressure (bar)	Particle Area (mm^2)	Bubble Area (mm^2)	Total Area (mm^2)	ε
0.25	8.2378	0.3792	8.617	0.044
0.50	7.3339	1.2831	8.617	0.149
0.75	7.2585	1.3585	8.617	0.158
1.00	7.1217	1.4953	8.617	0.174

Pressure (bar)	Particle Area (mm^2)	Bubble Area (mm^2)	Total Area (mm^2)	ε
0.25	8.3144	0.3026	8.617	0.035
0.50	7.9883	0.6287	8.617	0.073
0.75	7.9562	0.6608	8.617	0.077
1.00	7.8385	0.7786	8.617	0.090

It can be seen clearly that the void fraction of the bubbling bed increases with increased air pressure. Higher air pressure will provide more energy to push the particle upward and makes the bubble grow bigger. Thus the voidage is higher.

When sand is used as bed particles, the void fraction is bigger since its size and density is smaller than that of urea granules. At a similar pressure, the air will push the smaller particles upward more than the bigger particles since it can be easily fluidized.

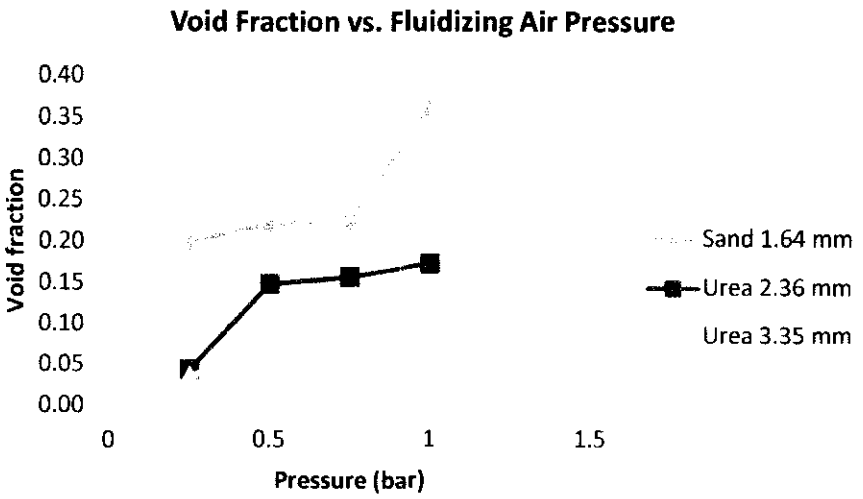

4.2 Bed Expansion, δ

The data for bed expansion is shown in Table 5-7.

Pressure (bar)	H_{mf} (cm)	H (cm)	δ
0.25	9.60	9.70	0.010309
0.50	9.60	10.80	0.111111
0.75	9.60	13.40	0.283582
1.00	9.60	16.91	0.432289

Pressure (bar)	H_{mf} (cm)	H (cm)	δ
0.25	8.90	9.00	0.011111
0.50	8.90	9.20	0.032609
0.75	8.90	10.20	0.127451
1.00	8.90	10.48	0.150763

Pressure (bar)	H_{mf} (cm)	H (cm)	δ
0.25	8.84	8.94	0.011186
0.50	8.84	9.14	0.032823
0.75	8.84	9.20	0.039130
1.00	8.84	9.95	0.111558

An increase in air pressure causes the bed expansion to increase. This is because the increasing pressure shoves the particle higher and makes the bed of particles expand more. Therefore bed expansion increases with pressure.

Bed expansion is higher for smaller particles and lower for the bigger particles. This is because sand is smaller and lighter compared to urea; a similar air pressure can make it fluidized and expand more.

The knowledge of the bed expansion is very important for modeling and design of fluidized beds. This information is required for an industrial designer for the case to establish the best possible position for a heat exchanger in fluidized bed reactors and determine the height of freeboard in order to avoid unnecessary loss of solids.

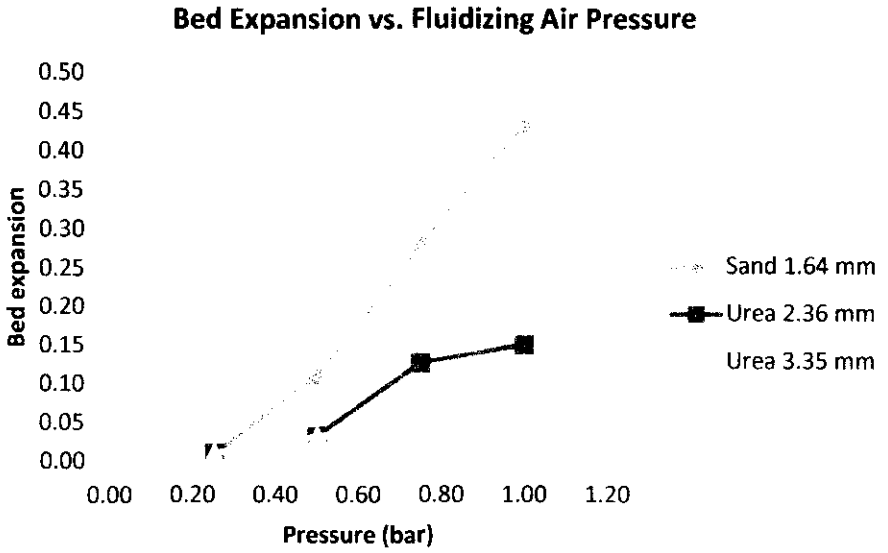

4.3 Bubble Diameter

The bubble diameter inside the bed is measured across the bed height and the results are shown in Figure 14-16. For the bed of sand particles at 0.25 bar, bubble is formed at 0 cm to 4.5 cm. At 0.5 bar, bubble is formed at 0 cm to 7 cm and its diameter is bigger. At 0.75 bar and 1 bar, bubbles are formed at 0 cm to 10.5 cm and the diameter is biggest at 1 bar.

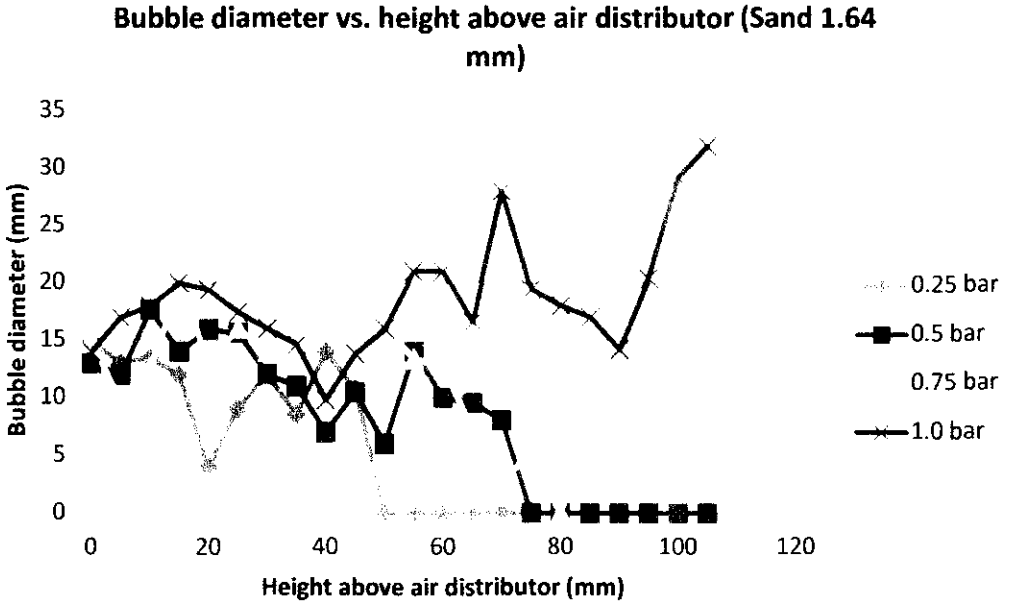

For the bed of urea granules of 2.36 mm-diameter, at 0.25 bar, bubble is formed at 0 cm to 1 cm. At 0.5 bar, bubble is formed at 0 cm to 3 cm and its diameter is bigger. At 0.75 bar, bubble is formed at 0 cm to 4 cm and its diameter is much bigger. At 1 bar, bubble is formed at 0 cm to 10.5 cm and the diameter is the biggest.

For the bed of urea granules of 3.35 mm-diameter, at 0.25 bar, a very small bubble is formed at 0 cm height. At 0.5 bar, bubble is formed at 0 cm to 1 cm and its diameter is bigger. At 0.75 bar, bubble is formed at 0 cm to 2.5 cm but its diameter is smaller. At 1 bar, bubble is formed at 0 cm to 9.5 cm and the diameter is the biggest compared to the other.

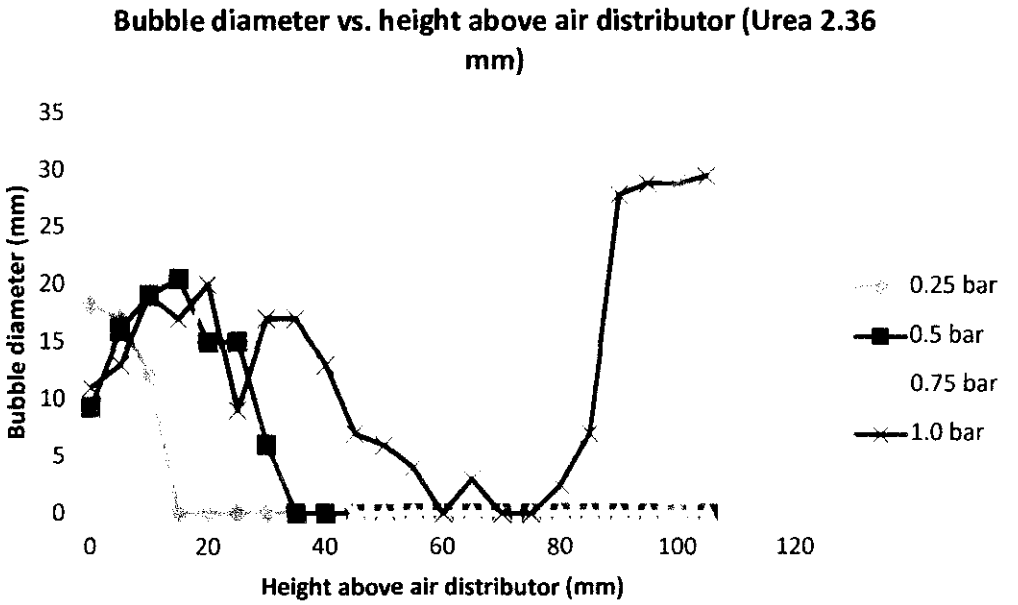

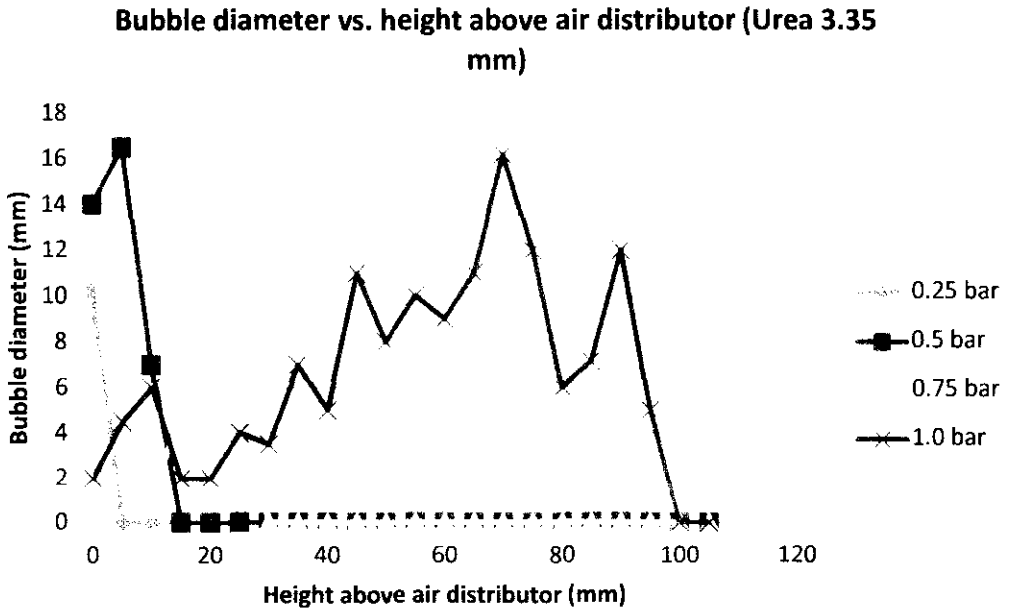

It is observed that bubble size increases with pressure and with height above the distributor. However, bubbles in bubbling fluidized bed can be irregular in shape and vary in size. As the bubbles form near the distributor and rise in a bubbling fluidized

bed, they grow up due to coalescence and split due to instabilities at the bubble boundary.

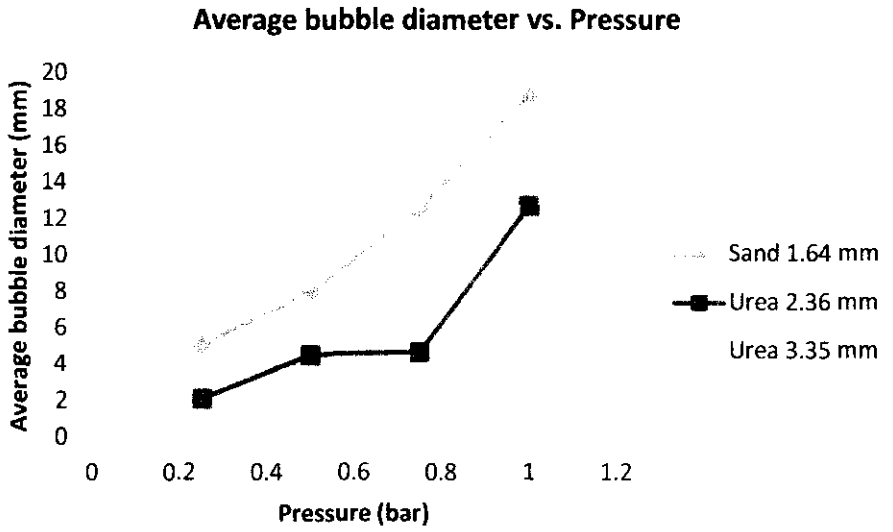

The average bubble diameter is calculated so that the effect of particle size can be evaluated. In Figure 17, it is observed that smaller bubbles are formed in the bed of urea compared to the bed of sand. This is because urea granules are bigger and have higher caking tendency. It means that urea tends to stick together and make it harder for formation of a big bubble compared to the bed of sand particles.

CHAPTER 5

CONCLUSION & RECOMMENDATION

In a conclusion, the hydrodynamic behavior which is described as void fraction, bed expansion and bubble diameter in fluidized bed processing is studied. The void fraction of the bubbling bed increases with increased air pressure. Higher air pressure will provide more energy to push the particles upward and makes the bubble grow bigger. Thus the voidage is higher.

The void fraction for the bed of sand is bigger since the particles are smaller than urea granules. At a similar pressure, the air will push the smaller particles upward more than the bigger particles since it can be easily fluidized.

An increase in air pressure causes the bed expansion to increase. This is because the increasing pressure shoves the particle higher and makes the bed of particles expand more. Therefore bed expansion increases with pressure.

Bed expansion is higher for smaller particles and lower for the bigger particles. This is because sand is smaller and lighter compared to urea; a similar air pressure can make it fluidized and expand more.

It is observed that bubble size increases with pressure and with height above the distributor. However, bubbles in bubbling fluidized bed can be irregular in shape and vary in size. As the bubbles form near the distributor and rise in a bubbling fluidized bed, they grow up due to coalescence and split due to instabilities at the bubble boundary.

The average bubble diameter is calculated so that the effect of particle size can be evaluated. It is observed that smaller bubbles are formed in the bed of urea compared to the bed of sand. This is because urea granules are bigger and have higher caking tendency. It means that urea tends to stick together and make it harder for formation of a big bubble compared to the bed of sand particles.

The results obtained are in good agreement with the previous works done by Piepers et al. (1984), Wiman and Almstedt (1998), and Olowson and Almstedt (1990) although the type and size of the particle and pressure range used in each study are different.

However, the range of data collected in this experiment is very small due to the limitation of the fluidized bed equipment itself. It is recommended that the equipment to be modified to withstand higher operating pressure, so that the hydrodynamic behavior of particles at elevated pressure can be observed and compared with the existing findings.

The flow rate of air should be varied so that the minimum fluidization velocity can be calculated and compared with theoretical value. Distributor plate with different hole size and arrangement can be used so the that the effect of distributor plate design can be studied.

REFERENCES

Bahman, Z. N., (2007). "Effect of process variables on the caking tendency of prilled urea in the warehouse of urea production plant". *Journal of the University of Chemical Technology and Metallurgy,* 42, 1, 45-50.

Boerefijn, R., & Ghadiri, M., (1998). "High speed video image analysis of flow of fine particles in fluidised bed jets". *The Institute of Particle Science & Engineering.* Adv. Powder Technol. 9, 229-243.

Breault, R. W., & Mathur, V. K. (1989). High-velocity fluidized-bed hydrodynamic modeling. 2. circulating bed pressure drop modeling. *Industrial & Engineering Chemistry Research, 28*(6), 688-693.

Cho, Y. J., Park, H. Y., Kim, S. W., Kang, Y., & Kim, S. D. (2002). Heat transfer and hydrodynamics in two- and three-phase inverse fluidized beds. *Industrial & Engineering Chemistry Research, 41*(8), 2058-2063.

Davies R.M. & Taylor G.I., (1950). "The mechanics of large bubbles rising through extended liquids and through liquids in tubes", *Proc. Roy. Soc.*, A200, 375.

Geldart D., (1973). "Types of Gas Fluidization", *Powder Technology.* 7, 285-292.

Geldart D., (1978). "Homogenous Fluidization in Fine Powder Using Various Gases and Pressures", *Powder Technology.* 19, 133-136.

Hamzehei, M., Rahimzadeh, H., & Ahmadi, G. (2010). Computational and experimental study of heat transfer and hydrodynamics in a 2D Gasâ^'Solid fluidized bed reactor. *Industrial & Engineering Chemistry Research, 49*(11), 5110-5121.

Hamzehei, M., & Rahimzadeh, H. (2009). Experimental and numerical study of hydrodynamics with heat transfer in a Gasâ^'Solid fluidized-bed reactor at

different particle sizes. *Industrial & Engineering Chemistry Research, 48*(6), 3177-3186.

Hesketh, R.P., Slater, C.S., Farrell, S. & Carney, M., (2002). "Fluidized Bed Polymer Coating Experiment," *Chem. Eng. Ed.* 36(2) 138.

Kato, K. & Wen, C.Y., (1969). "Bubble assemblage model for fluidized bed catalytic reactors", *Chem. Eng. Sci.* 24, 1351-69.

Leva M., (1959). Fluidization, McGraw-Hill, New York.

Pata, J., & Hartman, M., (1978). "Minimum fluidization velocities of lime and limestone particles". *Ind. Eng. Chem. Process Des. Dev.,* Vol. 17, No. 3.

Ren, B., Zhong, W., Zhang, Y., Jin, B., Wang, X., Tao, H., et al. (2010). Investigation on flow patterns and transitions in a multiple-spouted bed. *Energy Fuels, 24*(3), 1941-1947.

Renganathan, T. & Krishnaiah, K., (2005). "Voidage characteristics and prediction of bed expansion in liquid–solid inverse fluidized bed". *Chemical Engineering Science,* 2545 – 2555.

Shen, L., Johnsson, F., & Leckner, B., (2004). "Digital image analysis of hydrodynamics two-dimensional bubbling fluidized beds". *Chemical Engineering Science, 59*(13), 2607-2617.

Sidorenko, I., & Rhodes, M. J., (2003). "Pressure Effects on Gas-Solid Fluidized Bed Behavior". *International Jurnal of Chemical Reactor Engineering.*

Subramanian, G., Turton, R., Sheluker, S., Flemmer, L., (2003). Effect of tablet deflectors in the draft tube of fluidized/spouted bed coaters. *Industrial & Engineering Chemistry Research,* Vol. 42, 2470 - 2478.

Vijaya Lakshmi, A. C., Balamurugan, M., Sivakumar, M., Newton Samuel, T., & Velan, M. (2000). Minimum fluidization velocity and friction factor in a liquid-

solid inverse fluidized bed reactor. *Bioprocess and Biosystems Engineering, 22*(5), 461-466.

Vunjak-Novakovic, G., Vukovic, D. V., & Littman, H., (1987). Hydrodynamics of turbulent bed contactors. 2. pressure drop, bed expansion, and minimum fluidizing velocity. *Industrial & Engineering Chemistry Research, 26*(5), 967-972.

Wang, J., Ren, C., Yang, Y., & Hou, L. (2009). Characterization of particle fluidization pattern in a gas solid fluidized bed based on acoustic emission (AE) measurement. *Industrial & Engineering Chemistry Research, 48*(18), 8508-8514.

Wen C.Y. & Yu Y.H., (1966). "A Generalized Method for Predicting the Minimum Fluidization Velocity", *American Institute of Chemical Engineering Journal,* 12, 610-612.

Whittman, C. V., & Ademoyega, B. O. (1987). Hydrodynamic changes and chemical reaction in a transparent two-dimensional cross-flow electrofluidized bed. 1. experimental results. *Industrial & Engineering Chemistry Research, 26*(8), 1586-1593.

Wiman, J., & Almstedt, A. E. (1998). Influence of pressure, fluidization velocity and particle size on the hydrodynamics of a freely bubbling fluidized bed. *Chemical Engineering Science, 53*(12), 2167-2176.

APPENDICES

1. Bed expansion calculation for sand 1.64 mm

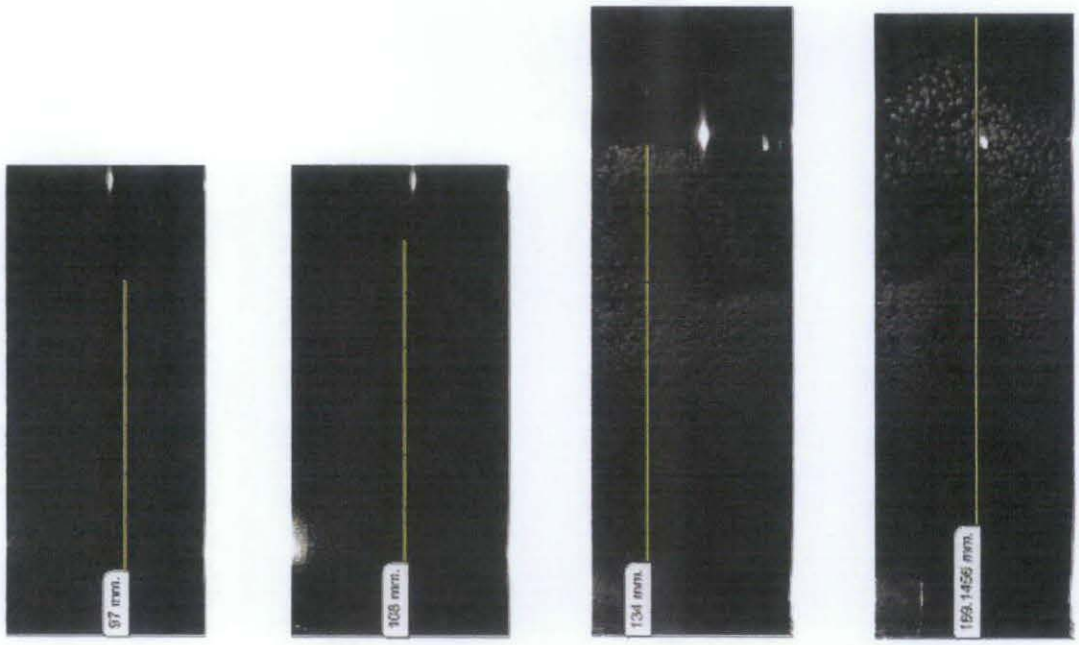

Figure 18: Sand 1.64 mm bed height, H at different pressure; (a) 0.25 bar (b) 0.5 bar (c) 0.75 bar (d) 1 bar

Height at minimum fluidization, H_{mf} = 9.6 cm

$$At\ P = 0.25\ bar, \quad \delta = \frac{H - H_{mf}}{H} = \frac{(9.7 - 9.6)cm}{9.7\ cm} = 0.010309$$

$$At\ P = 0.5\ bar, \quad \delta = \frac{H - H_{mf}}{H} = \frac{(10.8 - 9.6)cm}{10.8\ cm} = 0.111111$$

$$At\ P = 0.75\ bar, \quad \delta = \frac{H - H_{mf}}{H} = \frac{(13.4 - 9.6)cm}{13.4\ cm} = 0.283582$$

$$At\ P = 1\ bar, \quad \delta = \frac{H - H_{mf}}{H} = \frac{(16.91 - 9.6)cm}{16.91\ cm} = 0.432289$$

2. Bed expansion calculation for urea 2.36 mm

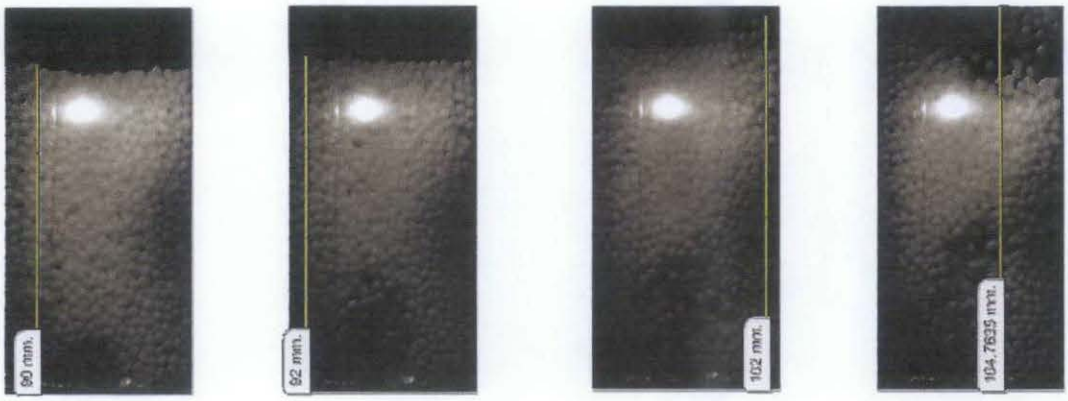

Figure 19: Urea 2.36mm bed height, H at different pressure; (a) 0.25 bar (b) 0.5 bar (c) 0.75 bar (d) 1 bar

Height at minimum fluidization, H_{mf} = 8.9 cm

$$At\ P = 0.25\ bar, \quad \delta = \frac{H - H_{mf}}{H} = \frac{(9.0 - 8.9)cm}{9.0\ cm} = 0.011111$$

$$At\ P = 0.5\ bar, \quad \delta = \frac{H - H_{mf}}{H} = \frac{(9.2 - 8.9)cm}{9.2\ cm} = 0.032609$$

$$At\ P = 0.75\ bar, \quad \delta = \frac{H - H_{mf}}{H} = \frac{(10.2 - 8.9)cm}{10.2\ cm} = 0.127451$$

$$At\ P = 1\ bar, \quad \delta = \frac{H - H_{mf}}{H} = \frac{(10.48 - 8.9)cm}{10.48\ cm} = 0.150763$$

3. Bed expansion calculation for urea 3.35 mm

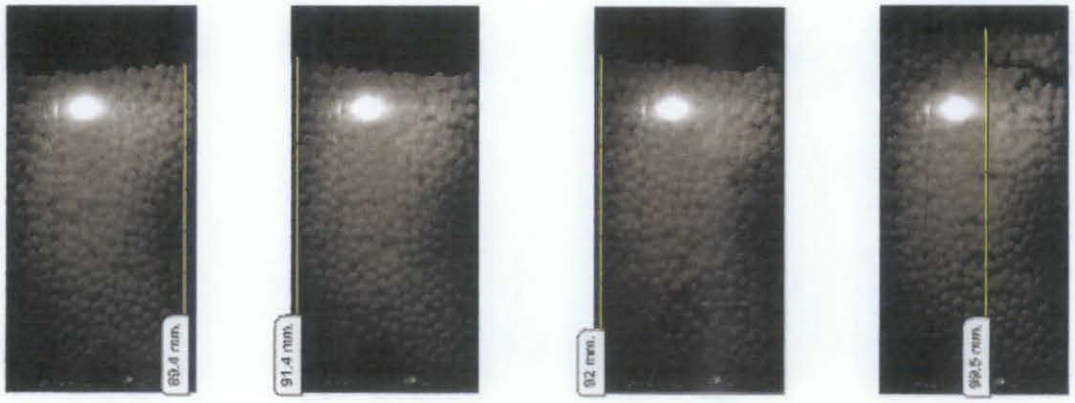

Figure 20: Urea 3.35mm bed height, H at different pressure; (a) 0.25 bar (b) 0.5 bar (c) 0.75 bar (d) 1 bar

Height at minimum fluidization, H_{mf} = 8.84 cm

$$At\ P = 0.25\ bar, \quad \delta = \frac{H - H_{mf}}{H} = \frac{(8.94 - 8.84)cm}{8.94\ cm} = 0.011186$$

$$At\ P = 0.5\ bar, \quad \delta = \frac{H - H_{mf}}{H} = \frac{(9.14 - 8.84)cm}{9.14\ cm} = 0.032823$$

$$At\ P = 0.75\ bar, \quad \delta = \frac{H - H_{mf}}{H} = \frac{(9.2 - 8.84)cm}{9.2\ cm} = 0.039130$$

$$At\ P = 1\ bar, \quad \delta = \frac{H - H_{mf}}{H} = \frac{(9.95 - 8.84)cm}{9.95\ cm} = 0.111558$$

4. Measurement of bubble diameter for bed of sand 1.64 mm

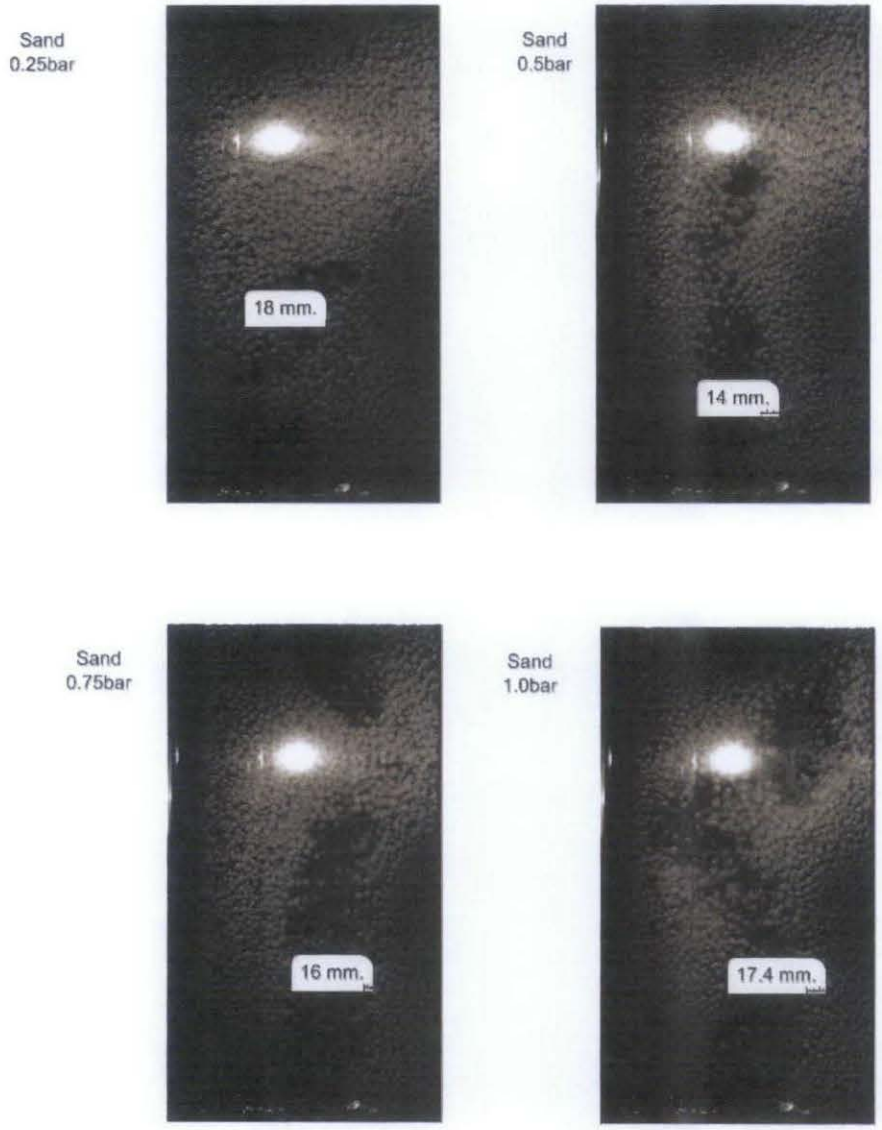

Figure 21: Bubble diameter for bed of sand 1.64 mm at different pressure

Height above air distributor (mm)	Pressure (bar)			
	0.25	0.50	0.75	1.00
	Bubble diameter (mm)			
0	15.00	13.00	15.00	14.00
5	13.00	12.00	9.60	17.00
10	13.50	17.70	12.40	18.00
15	12.00	14.00	20.00	20.00
20	4.00	16.00	13.00	19.40
25	9.00	15.60	16.00	17.40
30	12.00	12.00	14.00	16.00
35	8.50	11.00	18.60	14.60
40	14.00	7.00	16.40	9.80
45	10.80	10.50	14.00	13.80
50	0.00	6.00	16.00	16.00
55	0.00	14.00	13.40	21.00
60	0.00	10.00	12.60	21.00
65	0.00	9.50	7.20	16.60
70	0.00	8.00	3.00	28.00
75	0.00	0.00	5.00	19.40
80	0.00	0.00	0.00	18.00
85	0.00	0.00	7.80	17.00
90	0.00	0.00	13.60	14.20
95	0.00	0.00	13.00	20.40
100	0.00	0.00	14.60	29.20
105	0.00	0.00	21.60	32.00

5. Measurement of bubble diameter for bed of urea 2.36 mm

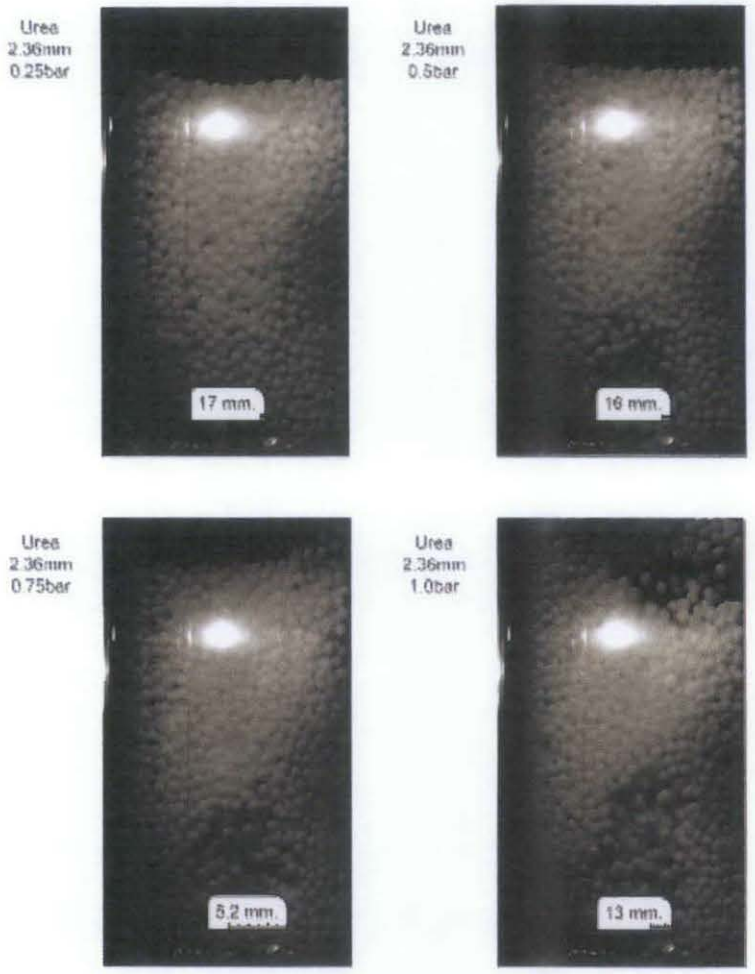

Figure 22: Bubble diameter for bed of urea 2.36 mm at different pressure

Height above air distributor (mm)	Pressure (bar)			
	0.25	0.50	0.75	1.00
	Bubble diameter (mm)			
0	18.20	9.28	6.00	11.00
5	17.00	16.00	5.20	13.00
10	12.00	19.00	10.50	19.00
15	0.00	20.50	11.50	17.00
20	0.00	15.00	21.00	20.00
25	0.00	15.00	22.00	9.00
30	0.00	6.00	18.00	17.00
35	0.00	0.00	6.80	17.00
40	0.00	0.00	3.00	13.00
45	0.00	0.00	0.00	7.00
50	0.00	0.00	0.00	6.00
55	0.00	0.00	0.00	4.00
60	0.00	0.00	0.00	0.00
65	0.00	0.00	0.00	3.00
70	0.00	0.00	0.00	0.00
75	0.00	0.00	0.00	0.00
80	0.00	0.00	0.00	2.50
85	0.00	0.00	0.00	7.00
90	0.00	0.00	0.00	27.85
95	0.00	0.00	0.00	28.85
100	0.00	0.00	0.00	28.80
105	0.00	0.00	0.00	29.50

6. Measurement of bubble diameter for bed of urea 3.35 mm

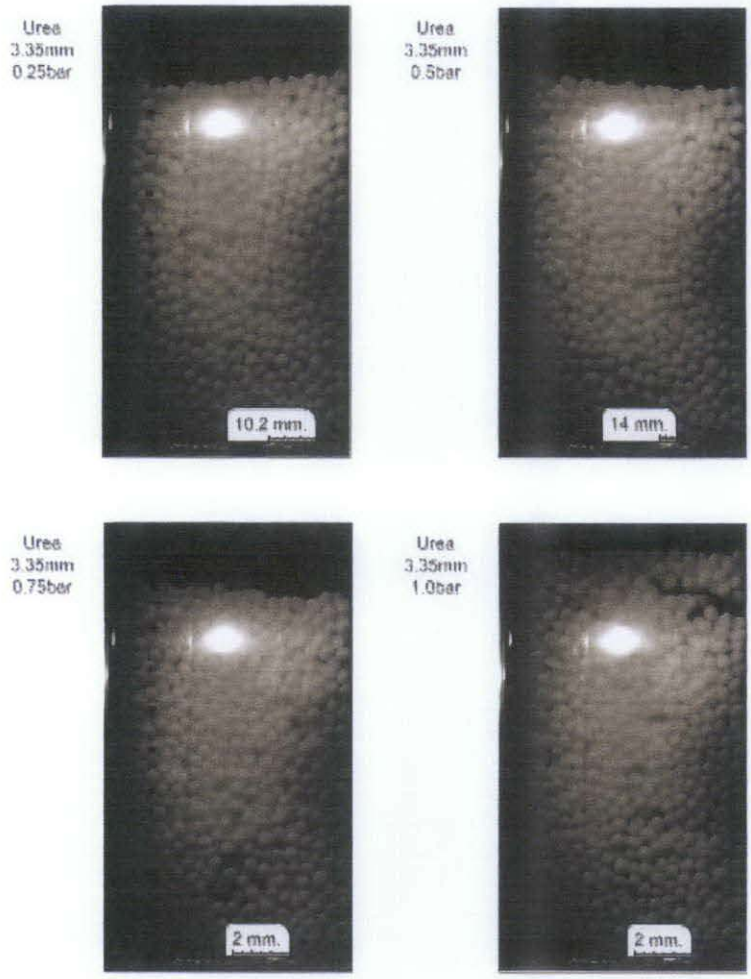

Figure 23: Bubble diameter for bed of urea 3.35 mm at different pressure

Height above air distributor (mm)	Pressure (bar)			
	0.25	0.50	0.75	1.00
	Bubble diameter (mm)			
0	10.20	14.00	2.00	2.00
5	0.00	16.50	4.00	4.50
10	0.00	7.00	1.20	6.00
15	0.00	0.00	5.00	2.00
20	0.00	0.00	10.00	2.00
25	0.00	0.00	6.00	4.00
30	0.00	0.00	0.00	3.50
35	0.00	0.00	0.00	7.00
40	0.00	0.00	0.00	5.00
45	0.00	0.00	0.00	11.00
50	0.00	0.00	0.00	8.00
55	0.00	0.00	0.00	10.00
60	0.00	0.00	0.00	9.00
65	0.00	0.00	0.00	11.00
70	0.00	0.00	0.00	16.20
75	0.00	0.00	0.00	12.00
80	0.00	0.00	0.00	6.00
85	0.00	0.00	0.00	7.14
90	0.00	0.00	0.00	12.00
95	0.00	0.00	0.00	5.00
100	0.00	0.00	0.00	0.00
105	0.00	0.00	0.00	0.00

7. Void fraction, ε for sand 1.64 mm

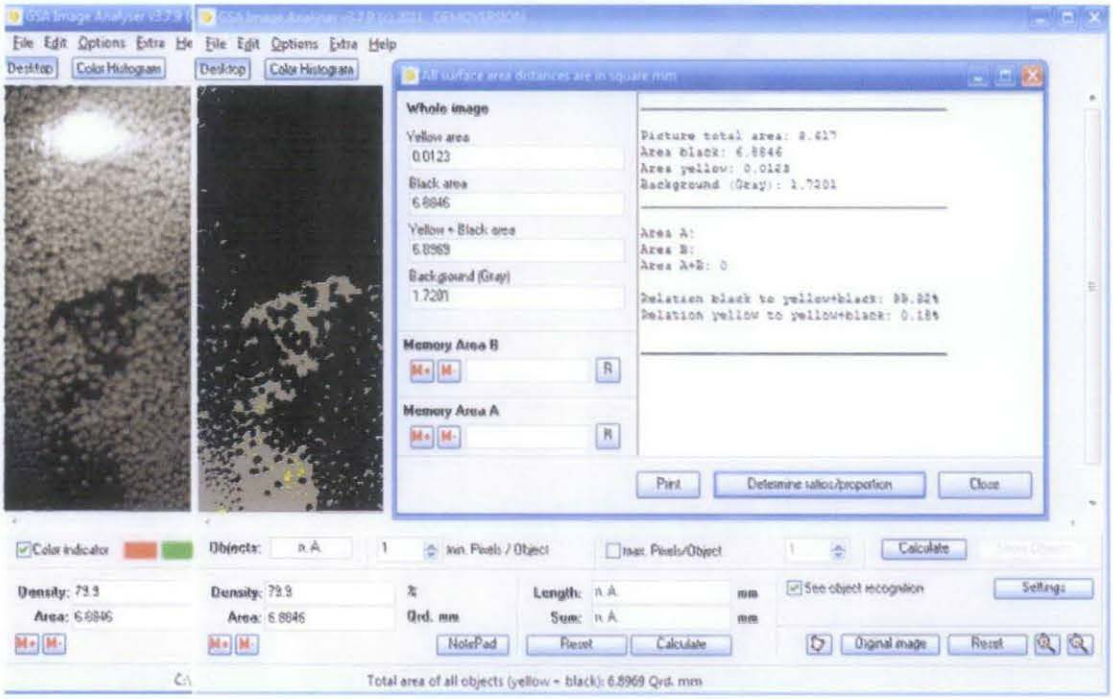

Figure 24: Void area at 0.25 bar

$$\varepsilon = \frac{gray\ projected\ area}{specified\ area} = \frac{bubble\ area}{total\ bed\ area} = \frac{1.7201}{1.7201+6.8969} = 0.200$$

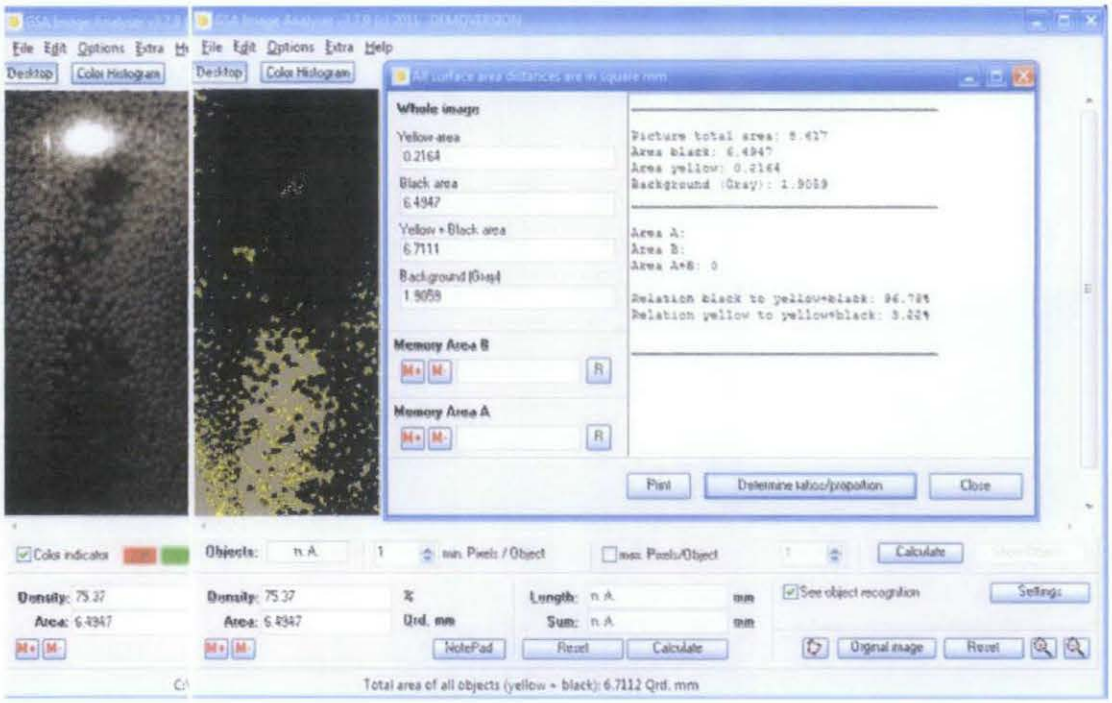

Figure 25: Void area at 0.5 bar

$$\varepsilon = \frac{gray\ projected\ area}{specified\ area} = \frac{bubble\ area}{total\ bed\ area} = \frac{1.9059}{1.9059 + 6.7111} = 0.221$$

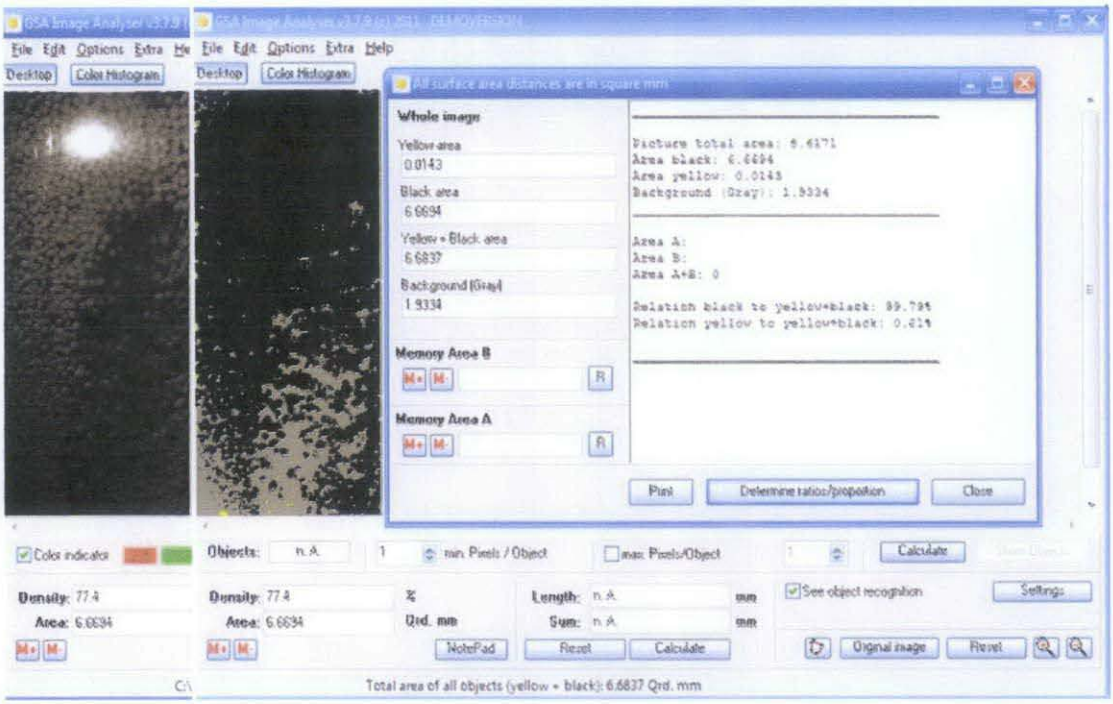

Figure 26: Void area at 0.75 bar

$$\varepsilon = \frac{gray\ projected\ area}{specified\ area} = \frac{bubble\ area}{total\ bed\ area} = \frac{1.9334}{1.9334 + 6.6837} = 0.224$$

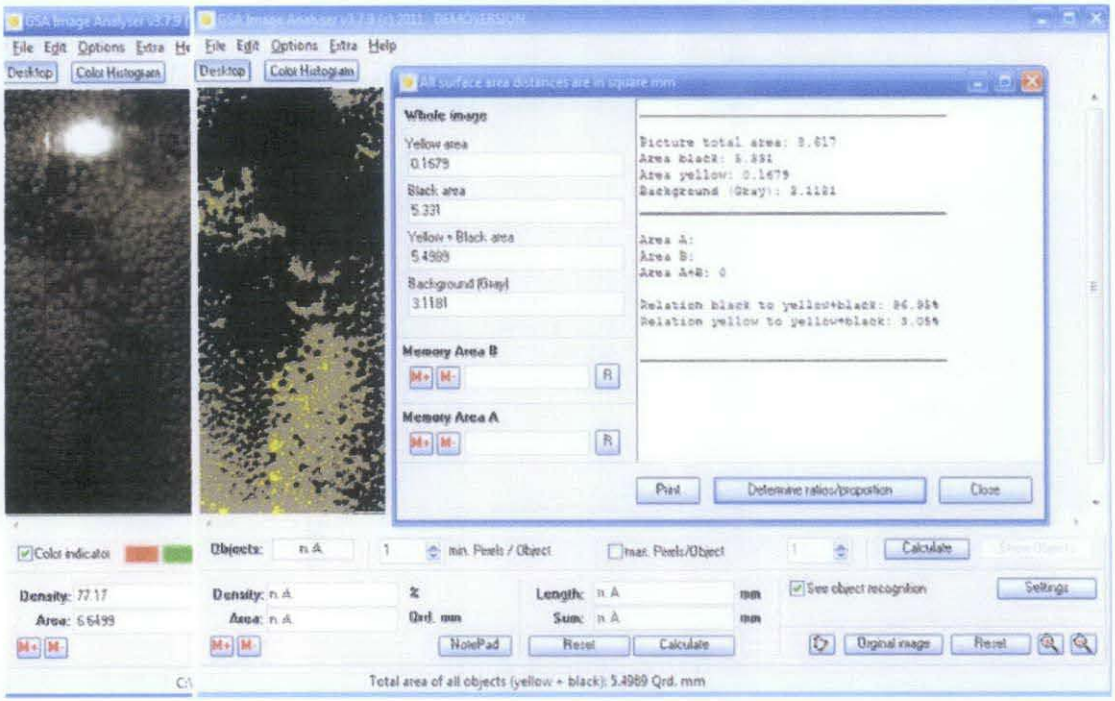

Figure 27: Void area at 1 bar

$$\varepsilon = \frac{gray\ projected\ area}{specified\ area} = \frac{bubble\ area}{total\ bed\ area} = \frac{3.1181}{3.1181 + 5.4969} = 0.362$$

8. Void fraction, ε for urea 2.36 mm

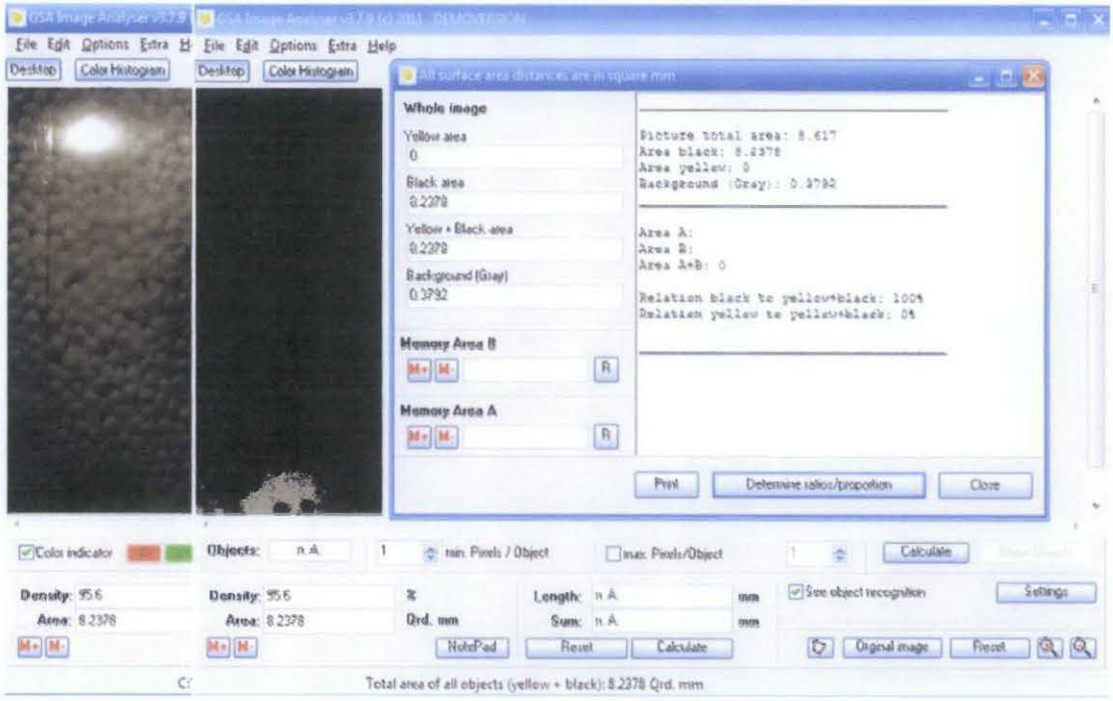

Figure 28: Void area at 0.25 bar

$$\varepsilon = \frac{gray\ projected\ area}{specified\ area} = \frac{bubble\ area}{total\ bed\ area} = \frac{0.3792}{0.3792 + 8.2378} = 0.044$$

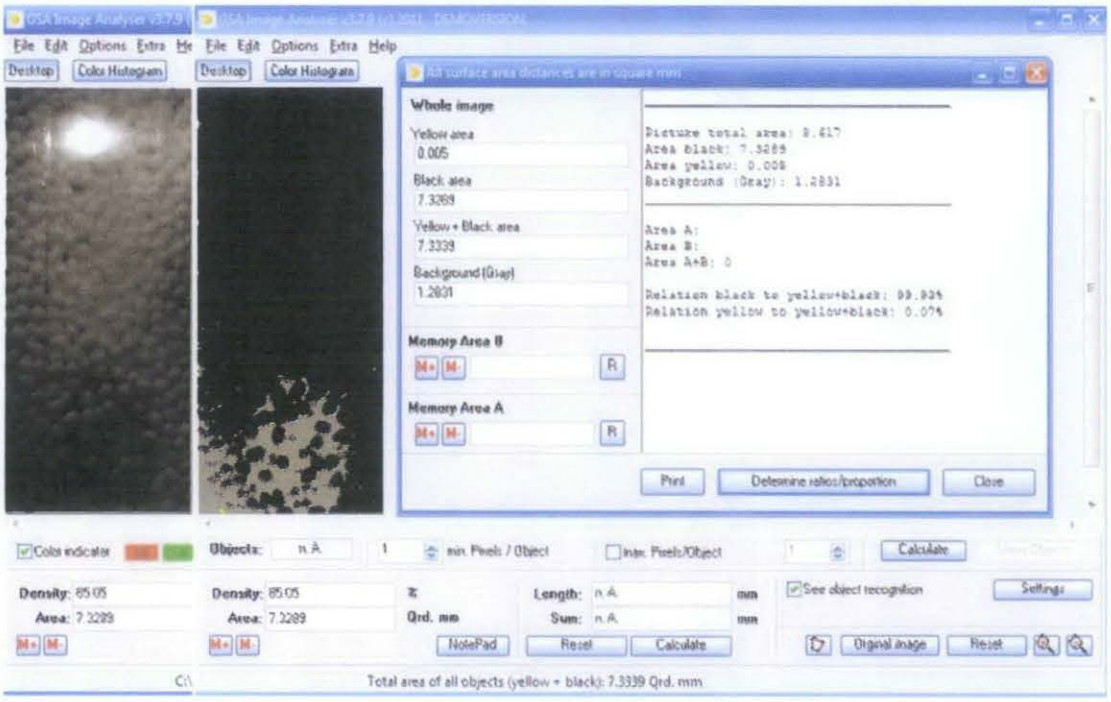

Figure 29: Void area at 0.5 bar

$$\varepsilon = \frac{gray\ projected\ area}{specified\ area} = \frac{bubble\ area}{total\ bed\ area} = \frac{1.2831}{1.2831 + 7.3339} = 0.149$$

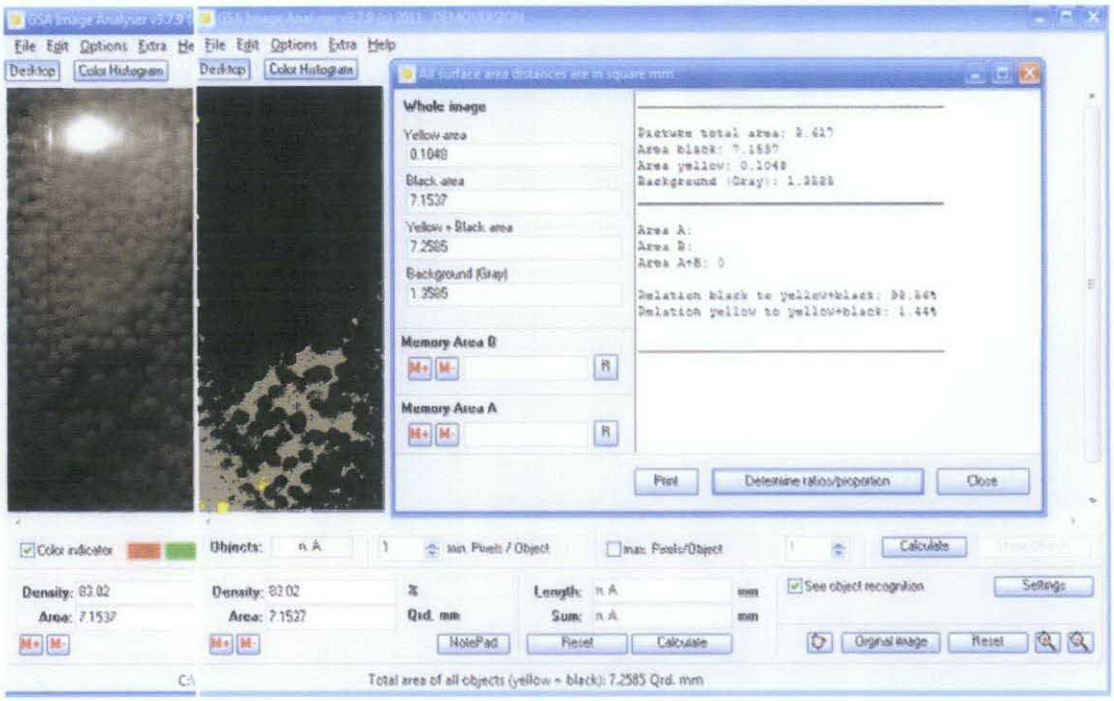

Figure 30: Void area at 0.75 bar

$$\varepsilon = \frac{gray\ projected\ area}{specified\ area} = \frac{bubble\ area}{total\ bed\ area} = \frac{1.3585}{1.3585 + 7.2585} = 0.158$$

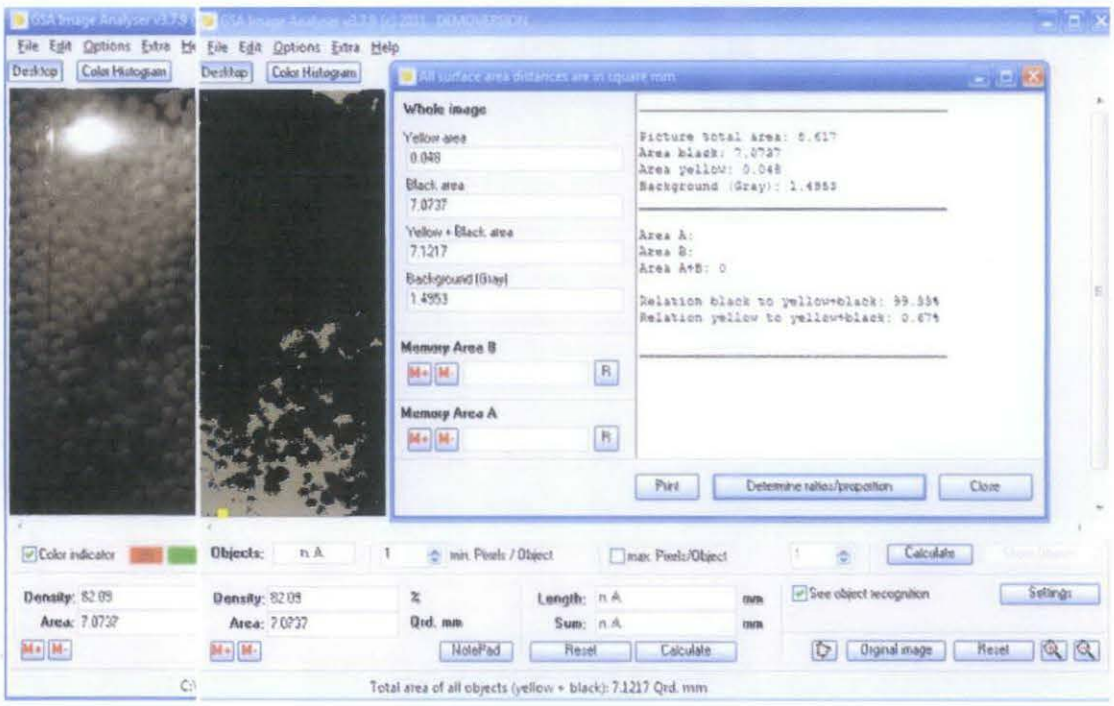

Figure 31: Void area at 1 bar

$$\varepsilon = \frac{gray\ projected\ area}{specified\ area} = \frac{bubble\ area}{total\ bed\ area} = \frac{1.4953}{1.4953 + 7.1217} = 0.174$$

9. Void fraction, ε for urea 3.35 mm

Figure 32: Void area at 0.25 bar

$$\varepsilon = \frac{gray\ projected\ area}{specified\ area} = \frac{bubble\ area}{total\ bed\ area} = \frac{0.3026}{0.3026 + 8.3144} = 0.035$$

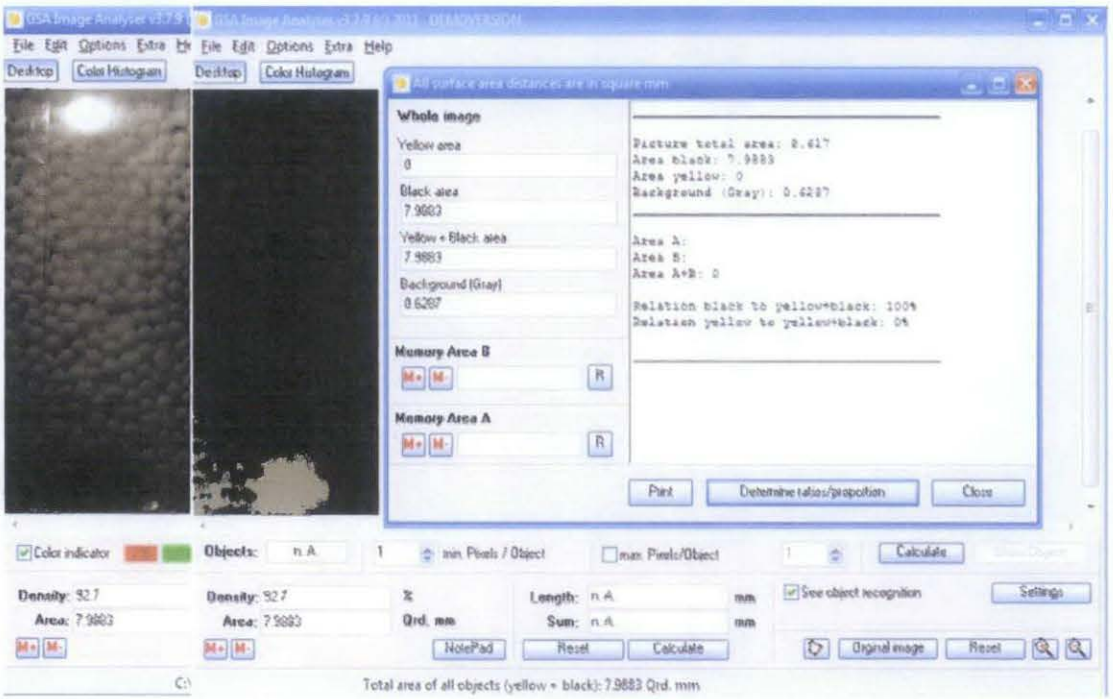

Figure 33: Void area at 0.5 bar

$$\varepsilon = \frac{gray\ projected\ area}{specified\ area} = \frac{bubble\ area}{total\ bed\ area} = \frac{0.6287}{0.6287 + 7.9883} = 0.073$$

Figure 34: Void area at 0.75 bar

$$\varepsilon = \frac{gray\ projected\ area}{specified\ area} = \frac{bubble\ area}{total\ bed\ area} = \frac{0.6608}{0.6608 + 7.9562} = 0.077$$

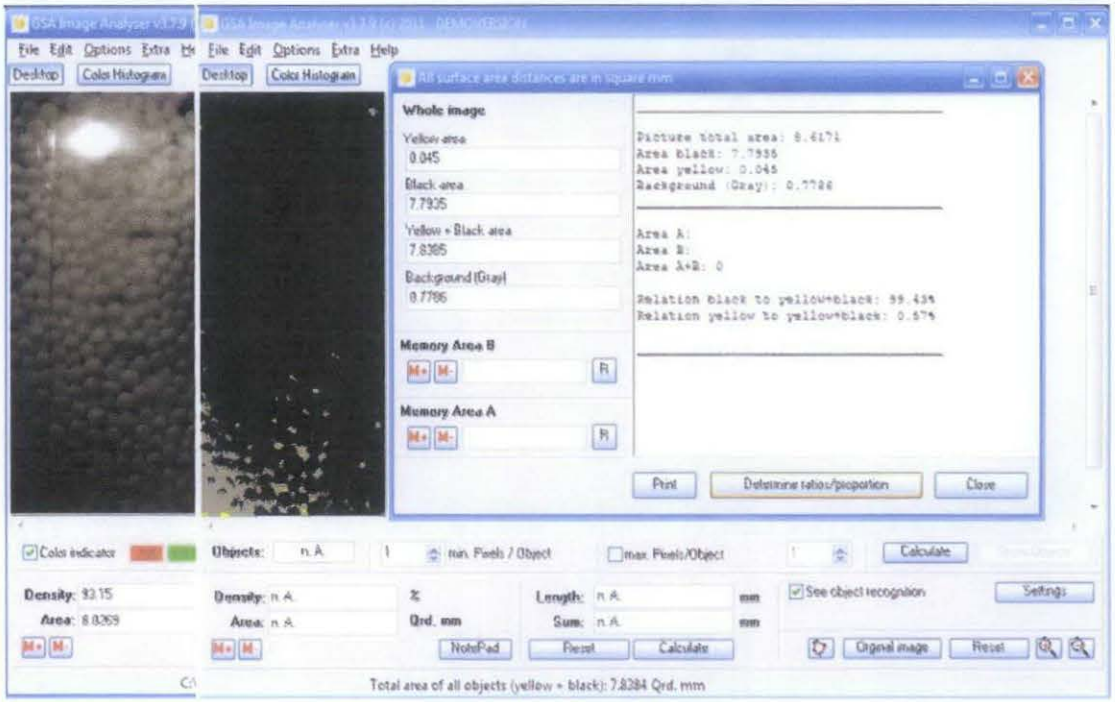

Figure 35: Void area at 1 bar

$$\varepsilon = \frac{gray\ projected\ area}{specified\ area} = \frac{bubble\ area}{total\ bed\ area} = \frac{0.7786}{0.7786 + 7.8385} = 0.090$$

10. Project Gantt Chart

Table 11: Project activities of FYP I

Project Phase / Activities	Week 1	2	3	4	5	6	7	8	9	10	11	12	13
Paper Work Submission													
1. Selection of FYP title													
2. Submission of Extended Proposal to Supervisor													
3. Submission of draft report to Supervisor													
4. Submission of final report to FYP Coordinator													
Briefing & Seminar													
1. FYP Briefing													
2. Seminar on "Research Methodology"													
3. Briefing on "Library Facilities & How to access Journals"													
4. Briefing on "Risk Assessment/ Lab Safety/ Rules & Regulations"													
Project Work													
1. Develop objective & scope of study													
2. Research & study the journals													
3. Literature review													
4. Identify experimental parameters													
5. Develop methodology of experiment													
Presentation													
Oral Proposal Defense													

Table 12: Project activities of FYP II

Project Phase / Activities	Week 1	2	3	4	5	6	7	8	9	10	11	12	13	14
1. Project work continues														
2. Submission of Progress Report														
3. Project work continues														
4. Poster Presentation														
5. Submission of Draft Report														
6. Submission of Dissertation (Softbound)														
7. Submission of Technical Paper														
8. Oral Presentation														
9. Submission of Project Dissertation (Hardbound)														